Ph.D. Dissertation in Agricultural Biotechnology

Structural studies on the assembly process of nuclear lamins by a mutation and phosphorylation

돌연변이와 인산화에 의한 핵 라민의 조립과정에 대한 구조적 연구

February 2023

The Graduate School
Seoul National University
Department of Agricultural Biotechnology
Food science and Biotechnology Major

Soyeon Jeong

Structural studies on the assembly process of nuclear lamins by a mutation and phosphorylation

Nam-Chul Ha

Submitting a Ph.D. Dissertation
in Agricultural Biotechnology

February 2023

The Graduate School
Seoul National University
Department of Agricultural Biotechnology
Food Science and Biotechnology Major

Soyeon Jeong

Confirming the Ph.D. Dissertation written by
Soyeon Jeong
February 2023

Chair _____(Seal)

Vice Chair _____(Seal)

Examiner _____(Seal)

Examiner _____(Seal)

Examiner _____(Seal)

Abstract

Structural studies on the assembly process of nuclear lamins by a mutation and phosphorylation

Soyeon Jeong
Food Science and Biotechnology Major
Department of Agricultural Biotechnology
The Graduate School
Seoul National University

Intermediate filament lamins in the cell nucleus form a three-dimensional meshwork that maintains the shape of the nucleus and offers a framework against external mechanical stress. The nuclear lamin is crucial to maintain the life of a cell. Lamin has various laminopathies caused by genetic mutations, of which the gene mutation of S143F has caused phenotypes characterized by both progeria and muscular dystrophy. This study determined the crystal structure of the lamin A/C fragment harboring the S143F mutant. The obtained structure revealed an X-shaped interaction between the tetrameric units in the crystals, potentiated by the hydrophobic interactions of the mutated Phe143 residues. Subsequent studies indicated that the X-shaped interaction between the filaments is crucial for disrupting the normal lamin meshwork. These results suggest the assembly mechanism of the 3-D meshwork and

provide a molecular framework for understanding the aging process by nuclear deformation.

Nuclear lamins maintain the nuclear envelope structure by forming long, linear filaments via two alternating molecular arrangements of coiled-coil dimers, known as A11 and A22 binding modes. The coupling between the coiled-coil dimer that binds to A11 and A22 during the lamin tetramer formation produces another parallel head-to-tail interaction between coil 1a and the C-terminal region of coil 2, called the ACN interaction. During mitosis, phosphorylation in the lamin N-terminal head region by the cyclin-dependent kinase (CDK) complex triggers the depolymerization of lamin filaments, but the associated molecular-level mechanisms remain unknown. This study revealed that phosphorylation by the CDK1 complex promotes the disassembly of lamin filaments by directly interfering with the ACN interaction between coil 1a and the C-terminal portion of coil 2 using purified proteins. Furthermore, it was observed that this interaction was disrupted as a result of alteration in the ionic interactions between coil 1a and coil 2. In addition, the disassembly mechanism of CDK1-dependent lamin filaments was presented in combination with molecular modeling.

The L59R mutation of lamin-induced laminopathy causes cardiomyopathy and Malouf syndrome phenotypes in muscular dystrophy. It was confirmed through previous experiments that this gene mutation changes the

stability of coil 1a to strongly induce ACN interaction, which is strong enough to restrain attempts to disperse lamin by kinase. This research screened a natural compound that inhibits ACN interaction and selected the flavonoids morin, baicalein, fisetin, and apigenin. Molecular docking and molecular dynamics simulations were used to explain their molecular mechanisms. Furthermore, HT1080 cell-based assays showed the possibility of using flavonoids as effective molecules for abnormal interactions of lamin A. These results show the possibility that flavonoids are directly involved in both the inhibition of protein binding and antioxidant function in the genetic diseases of lamin and can be used as a therapeutic agent.

Keywords: Intermediate filament, nuclear lamin A/C, laminopathies, phosphorylation, crystal structure, flavonoid

Student Number: 2017-29613

Table of Contents

List of Figures

List of Tables

Chapter 1.

Background

1.1. The role of nuclear lamins in cells

1.1.1. Expression of nuclear lamins and gene organization

Nuclear lamins contribute to the structural properties of the nuclear envelope and are classified as type V intermediate filament proteins based on the structure and sequence homogeneity (Herrmann and Aebi, 2000; Lazarides, 1980). The lamins are comprised of two major types: A-types and B-types. A-type lamins are encoded by LMNA and are classified into lamins A and C by alternative splicing. In contrast, B-type lamins, called lamins B1 and B2, are encoded by LMNB1 and LMNB2, respectively. (Machiels et al., 1996; McKeon et al., 1986). A-type lamins are expressed in most differentiated cell types, and B-type lamins are expressed in somatic cells. (Erber et al., 1999).

As a type V intermediate filament, nuclear lamins are characterized in three major parts: a central α-helical rod domain, an unstructured N-terminal head domain, and a C-terminal tail domain that includes a nuclear localization signal (NLS) sequence, an immunoglobulin-like domain (Ig-like domain), and a CAAX motif (C: Cysteine, A: aliphatic residue, and X: variable residue). (Stuurman et al., 1998). The central α-helical rod domain is subdivided into coil 1a, L1, coil 1b, L12, and coil 2. Coil 1b contains 42 amino acids over other intermediate filament types. By post-translational modification, these CAAX motif cleavages by ZMPTSTE24 and farnesylated at the cysteine residue. The B-types of lamin have this CAAX motif, but lamin A only has a CAAX motif in A-type lamins. (Beck et al., 1990).

1.1.2. Characteristic structural features of lamin

In vivo assembles of nuclear lamin revealed a meshwork of 3.5-nm-thick filament using cryo-electron tomography (Turgay et al., 2017). In particular, the lamin protein shown in the nuclear layer assembly mechanism is characterized by fibers formed based on the coiled-coil dimer. This fiber was organized by three main interactions: A11, A22, and ACN. The central rod domain of the lamin forms a parallel coiled-coil dimer called A11 interaction when two coiled-coil dimers are arranged antiparallel to the center of coil 1b. The antiparallel A11 interactions of two coiled-coil dimers are shown as crystal structures with a resolution of 3.2 Å (Ahn et al., 2019a). In the longitudinal interaction of the lamin, the tetramers are arranged antiparallel between coil2, which is called A22 interactions. It is called A22 interactions. Finally, the parallel head-to-tail overlapping the coil-coil dimers is called the ACN interaction in the lamin longitudinal assembly, which has been identified based on crosslink analysis studies (Stalmans et al., 2020; Vermeire et al., 2021).

Nuclear lamin has different properties due to several post-translational modifications, including farnesylation, phosphorylation, sumoylation, O-GlcNAcylation, acetylation, ubiquitination, and methylation (Murray-Nerger and Cristea, 2021). Among various PTMs, phosphorylation is directly related to the disassembly of nuclear lamin. In the early stages of mitosis, lamin phosphorylated by several kinases splits the meshwork structure and contributes to cell division. After mitosis completes, the nuclear mesh can be developed by the dephosphorylated lamin. LC-MS/MS analysis revealed about 92 phosphorylated sites, most of which are distributed at the N-terminal head domain and the C-

terminal tail domain of lamin. Cyclin-dependent kinase 1 (CDK1) and protein kinase C (PKC) drive the beginning of cell distribution, Ser22 and Ser392 residues are targeted by CDK1, and Ser340 residue is targeted by PKC. The mutational study in cells reveals the importance of these residues. Lamin-expressed cells with a mutation that cannot be phosphorylated cannot perform regular separation of the meshwork structure of the nuclear envelope and thus exhibit abnormal nuclear forms.

1.1.3. Lamins regulate nuclear mechanics

Since nuclear lamins are essential proteins that constitute the framework of the nucleus along the nuclear membrane, they contribute to the stability of the nucleus and its fundamental role in maintaining the spherical shape of the nucleus against mechanical stress. (Fedorchak et al., 2014; Swift et al., 2013). To date, both A-types and B-types of lamin proteins have been revealed to be linked to other cytoskeletal proteins via the linker of nucleoskeleton and cytoskeleton (LINC) complexes, contributing to maintaining cell stiffness and contractility (Vahabikashi et al., 2022).

The LINC complex consists of the SUN and Nesprin proteins located in the inner and outer membranes of the nucleus, respectively, with the same KASH domains. Within the nucleus, the SUN protein interacts with the lamin A network to transmit and receive signals; some interact with lamina-associated domains. Then, the linked nesprin interacts either directly or indirectly with other cytoskeletons outside the nucleus, helping to interact with the layers inside the nucleus. Specifically, Nesprin 1/2 is known to interact with F-actin, Nesperin3

with intermediate filaments localized in cytosol such as a Vimentin, and Nesprin 4 with microtubules. Thus, lamin localization inside the nucleus can be sensitive to mechanical stress outside the nucleus with the help of LINC. In addition, when the lamin protein was either knocked out or down within the cell, it exhibited that the cell nucleus was spherical in shape and disrupted the cell's overall shape and rigidity. (Osmanagic-Myers et al., 2015).

1.1.4. Lamins regulate chromatin organization and DNA damage and repair

The nuclear lamina consists of A- and B-types of lamin organized as a meshwork. Nuclear lamins also interact with a lamin-associated domain of genomes and chromosomes, where the contact sites with lamins are called lamina-associated domains (LADs). Heterochromatin was tethered with nuclear lamina through the protein of LADs, and the LADs embrace the 0.1−10 Mb area of the genome (Guelen et al., 2008). Chromatin immunoprecipitation (ChIp) assays reveal the LAD regions (Handoko et al., 2011). Nuclear lamins directly interact with LADs of chromatin while indirectly using the chromatin-binding protein. Generally, B-type lamin interacts with LADs via the Lamin B Receptor (LBP) and HP1α close to the nuclear peripheral. In contrast, A-type lamin interacts with LAP2α, Emerin, and BANF1 close to the nuclear inner membrane and even exists inside the nucleus. (Willaume et al., 2021).

Lamins interacting with chromatin are also related to DNA transcription, replication, and repair. The proportion of damaged DNA increased after studying

diseases related to lamin A deficiency, revealing that histones H2AX and γH2AX are related to lamin A. (Mahen et al., 2013). Furthermore, when a recovery system containing homologous recombination (HR) and non-homologous end junctions (NHEJ) is needed for DNA damaged by double-stranded breakage, lamin A is reportedly associated with proteins that are the substances of DNA repair.

1.2. Classification of laminopathies

Mutations in the genes of lamins cause serious diseases called laminopathies (Rankin and Ellard, 2006). Genetic mutations that cause classical laminopathies are mainly found in A-type lamins, while mutations cause other laminopathies in B-type lamins or incomplete processing of pre-lamin A and proteins that bind to lamin. Numerous gene mutations exist in laminopathies, and >400 mutations have been reported (Kochin et al., 2014). These mutations occur throughout the entire region of the lamin protein, resulting in muscular dystrophy, lipodystrophy, and aging-promoted disease.

1.2.1. Muscular dystrophy

Laminopathies, which mainly occur in cells that receive severe mechanical stress such as muscle cells, were first described as Emery–Dreifuss muscular dystrophy (EDMD) and include three categories: Autosomal dominant-EDMD (AD-EDMD), autosomal recessive-EDMD (AR-EDMD), and X-linked-EDMD (XL-EDMD). These EDMDs appear as loss of skeletal muscle in calves and arms near the shoulders in teenagers; moreover, there is a dilated cardiomyopathy effect without skeletal muscle that can cause heart problems (Fatkin et al., 1999).

1.2.2. Lipodystrophy

There are some gene mutations of lamins' Ig-like domain in adipose tissue, which is called Familial partial lipodystrophy; Dunnigan type (FPLD), especially p.R482Q/W gene mutation. (Bidault et al., 2011; Guillin-Amarelle et al., 2018).

This disease appears as abnormally distributed adipose tissue and accumulates in particular areas in early adulthood or childhood, resulting in insulin resistance and diabetes.

1.2.3. Hutchinson Gilford Progeria Syndrome (HGPS)

When the prelamin A transformed mature lamins after undergoing post-translational modification on the CaaX motif, endonuclease ZMPSTE24 was unable to produce a mature lamin, causing a deficient gene sequence encoding 50 amino acids, including the cleavage site. This caused the permanently farnesylated protein progerin generation, referred to as Hutchinson–Gilford Progeria Syndrome (HGPS) (Piekarowicz et al., 2019; Pollex and Hegele, 2004). HGPS is a well-known representative age-related segmental progeroid disease. A recent study revealed that the unprocessed C-terminal region of progerin atypical interaction with the Ig-like domain of mature lamin A leads to nuclear deformation (Lee et al., 2016). A flavonoid morin is managed as an inhibitor of unexpected binding (Ahn et al., 2021c).

1.3. Flavonoid

1.3.1. Classification of flavonoid

Flavonoids are natural phenolic compound that can be easily found in fruits and vegetables and consists of two aromatic rings and a pyran ring (Khan et al., 2021; Ramesh et al., 2021). There are 15 carbons located in the basic skeleton of flavonoids, consisting of C6-C3-C6. Two benzenic rings, A and B rings, are connected with the C ring as a closed pyran ring containing three carbons. These flavonoids are classified into six subclasses according to oxidation levels and the position to the linked B ring : flavone, flavonol, flavanol, isoflavone, flavanol, and anthocyanins. The isoflavone's C ring is connected to position 4 of the B ring, and the others five flavonoid subclasses' C ring is linked to position 3 of the B ring.

1.3.2. Flavonoid as an anti-aging agent

Flavonoids are mainly known for anti-oxidant properties and have polypharmacy activities containing anti-inflammatory, anti-diabetes, and anti-obesity activity (Fan et al., 2022; Rufino et al., 2021). Recent studies have shown that flavonoids have sufficient ability to anti-aging. Aging cells secrete an inflammatory substance called senescence-associated secretory phenotype (SASP) (Yousefzadeh et al., 2018). Among flavonoids, compounds with senolytic properties that directly remove aging cells and senostatic properties that inhibit SASPs are present. In addition, flavonoids inhibit cell aging in various ways, such as regulating the reactive oxygen species of aging cells or weakening the effect of UVC that damages DNA.

1.4. Purpose of Research

The nuclear lamin responsible for skeletal formation inside the cell nucleus plays an essential role in maintaining the nucleus's shape and protecting DNA. In addition, it communicates with other cytoskeleton proteins in the cytosol through nuclear transmembrane proteins to regulate the overall shape and whole-cell mechanics. Thus, when gene mutations called laminopathies occur, they create life-threatening diseases. This study presents an interpretation of the structure of lamin S143F, which has abnormal interactions with other filaments while assembling in a cell and investigates the reasons through the molecular mechanism. Furthermore, this study suggests the molecular mechanism of how phosphorylation operates lamin disassembly in mitosis. Finally, the inhibition candidate natural compound showed for the L59R mutation of lamin A, which has atypical stiffening interaction and is unable to dissolve in mitosis. This research aimed to contribute to understanding the molecular mechanism of laminopathies and provide insights into flavonoids as inhibitors.

Chapter 2.

Crystal structure of progeria mutant S143F lamin A/C and its implications for premature aging

Published in Communications Biology

Ahn, J.*, **Jeong, S.***, Kang, S. M., Jo, I., Park, B. J., & Ha, N. C. (2022). Crystal structure of progeria mutant S143F lamin A/C reveals increased hydrophobicity driving nuclear deformation. Communications biology, 5(1), 1-8.

***These authors contributed equally: Jinsook Ahn and Soyeon Jeong.**

2.1. Introduction

The nuclear lamina is mainly composed of intermediate filament (IF) lamins and forms a protein-made meshwork that maintains the nuclear shape (Aebi et al., 1986; Lopez-Soler et al., 2001; Stuurman et al., 1998). Lamins consist of an alpha-helical central rod domain, an N-terminal head region, and a C-terminal long tail region. The central alpha-helical rod domain of lamins is further divided into three subdomains, coil 1a, coil 1b, and coil 2, interrupted by linkers L1 and L12. Lamins belong to the type V IF family, distinguished from the cytosolic types of IF proteins, such as vimentin and keratin (Fuchs and Weber, 1994; Herrmann et al., 2007). The C-terminal tail region contains a nuclear localization signal and a globular Ig-like domain, which are unique features of lamins compared to cytosolic IF proteins (Ahn et al., 2021a; Krimm et al., 2002). Another feature of vertebrate lamins is the additional six-heptad repeats in the middle of the coil 1b regions (Ahn et al., 2019b; Bera et al., 2016; Chernyatina et al., 2015).

A recent in situ cryo-ET structure of lamin filament revealed a 3.5-nm-thick filamentous structure regularly decorated with Ig-like domains. The lamin filaments were significantly thinner than the cylindrical-shaped cytosolic types of IF proteins with a 10-nm diameter (Turgay et al., 2017; Turgay and Medalia, 2017). The basic building units of lamin filaments are coiled-coil dimers formed by parallel coiled-coil interactions between the central rod domains. The two basic building units are further assembled antiparallelly by overlapping the coil 1b regions, called the ‘A11 tetramer’, as a polymerization intermediate. The crystal structure of a long N-terminal fragment containing two-thirds of the central rod

domain of human lamin A/C visualized high-resolution features of the A11 tetramer, essentially formed by the A11 interaction (Ahn et al., 2020; Ahn et al., 2019b) (Eldirany et al., 2021b; Lilina et al., 2020). To longitudinally join the A11 tetramers, the other interaction, the so-called eA22 interaction, was necessary. The A22 interaction describes the antiparallel interaction between the coil 2 regions, including the adjacent coil 1a and L1 regions. According to the previously proposed assembly model (Ahn et al., 2019b), the alternative and mutual synergistic application of the A11 and A22 interactions to the essential building dimeric units created the 3.5-nm-thick filamentous structure of lamin A/C. In the filament formation process, the N- and C-terminal of lamin A/C overlap parallelly, and the lengths of the overlapped region were expected to be 6 nm (Makarov et al., 2019; Stalmans et al., 2020) by recent crosslinking data. Further studies are required to determine the exact overlapping length, which is critical for understanding filament formation at the molecular level.

The structural organization of intermediate filaments is essential in understanding IF-related human diseases. However, only a few mechanisms have been proposed to connect genetic mutations of IF proteins and human diseases structurally. Structural analysis of K1/K10 demonstrated that a single mutation of type I keratins alters the electrostatic surface potential of K1/K10 heterotetramers, which causes human diseases. S233L mutation in type I keratins increased hydrophobicity on the K1/K10 tetramer surface (Bunick and Milstone, 2017; Eldirany et al., 2019; Eldirany et al., 2021b). This aberrant extra hydrophobicity induced higher-order aggregation, resulting in epidermolytic palmoplantar keratoderma (Eldirany et al., 2019; Eldirany et al., 2021b). This mechanism shows

that only one residue changes in IF proteins significantly affects filament formation associated with the pathogenesis of human diseases.

Several genetic mutations of lamin A/C resulted in defects in the nuclear envelope, leading to progeroid syndrome or muscular dystrophies (Broers et al., 2006; Butin-Israeli et al., 2012; Marcelot et al., 2021; Muchir et al., 2004). The S143F mutation at LMNA exhibited mixed phenotypes of muscular dystrophy and progeroid syndrome with a deformed nuclear envelope structure, as observed in HGPS cells (Kandert et al., 2007; Kirschner et al., 2005; Shimi et al., 2010). Hutchinson Gilford progeria syndrome (HGPS) is caused by a dominant mutation at the splicing site in LMNA, resulting in the expression of progerin, whose C-terminal tail is altered from normal lamin A. Progerin remains farnesylated at the altered C-terminal end, unlike the mature form of wild-type lamin A/C (Marcelot et al., 2020). Many mechanisms have been proposed to connect genetic mutations and nuclear deformation structurally. The remaining farnesyl group was proposed as the main reason for the nuclear deformation induced by progerin (Gordon et al., 2012; Marcelot et al., 2020; Young et al., 2006). However, there were results that an aberrant additional interaction between the Ig-like domain and the distinct C-terminal region of progerin is critical for nuclear deformation (Ahn et al., 2021b; Kang et al., 2021; Lee et al., 2016).

This study determined the crystal structure of the long fragment of lamin A/C harboring the S143F mutation. Based on the crystal structure and subsequent biochemical studies, a molecular mechanism was proposed that accounts for nuclear deformation, the hallmark of progeroid syndromes, at the molecular level.

2.2. Materials and Methods

2.2.1. Plasmid construction

The plasmids expressed wild-type lamin fragments (residues 1-300 and residues 250-400), as previously reported (Ahn et al., 2019b). PCR-based site-directed mutagenesis was performed on the wild-type lamin fragment (residues 1-300) to overexpress the S143F mutant lamin fragment (residues 1-300). The resulting DNA was inserted into the pProEx-HTa vector (Thermo Fisher Scientific, MA, USA). The resulting plasmid was transformed into the Escherichia coli strain BL21 (DE3; Novagen, USA) or B834 (DE3; Novagen, USA) to obtain the selenomethionyl-labeled protein for crystallization.

2.2.2. Purification of the recombinant proteins

Transformed E. coli cells were cultured in 4 L of Terrific broth or M9 medium supplemented with L-(+)-selenomethionine at 37°C. Protein expression was induced by 0.5 mM IPTG at 30°C. After cell harvest by centrifugation, cells were resuspended in lysis buffer containing 20 mM Tris-HCl (pH 8.0), 150 mM NaCl, and 2 mM 2-mercaptoethanol. The cells were disrupted using a continuous-type French press (Constant Systems Limited, Daventry, UK) at 23 kpsi pressure, and the cell debris was removed by centrifugation at 19,000 x g for 30 min at 4°C, after which the supernatant was loaded onto cobalt-Talon affinity agarose resin (Qiagen, The Netherlands) in lysis buffer. The target protein was eluted with lysis buffer supplemented with 250 mM imidazole. The eluate was treated with TEV protease to cleave the hexaHis-tag and was then loaded onto a HiTrap Q column

(GE Healthcare, USA). A linear gradient of increasing NaCl concentration was applied to the HiTrap Q column. The protein fractions were applied onto a size exclusion chromatography column (HiLoad Superdex 200 26/600 column; GE Healthcare, California, USA) pre-equilibrated with lysis buffer.

2.2.3. Crystallization, structure determination, and analysis

The S143F mutant lamin 300 fragment (8 mg/ml) was crystallized in a precipitation solution containing 0.2 M Tris-HCl (pH 8.0), 0.1 M sodium citrate, and 18% PEG 400 using the hanging-drop vapor diffusion method at 16°C. Next, the crystals of the lamin fragment were briefly dipped in a cryoprotectant solution containing 20% galactose and were flash-frozen in a nitrogen stream at -173°C. The diffraction datasets were collected using an Eiger 9 M detector at Beamline 5C at PLS (Pohang, Republic of Korea) and were processed with the HKL2000 package (Otwinowski and Minor, 1997). The structure of the S143F mutant lamin fragment was determined using the molecular replacement method with MOLREP in the CCP4 package (Winn et al., 2011). The structure of the wild-type lamin 300 fragment (PDB code: 6JLB) was split into two parts (residues 67-145; 146-240) and was used as the search model for molecular replacement. The crystals belonged to space group P4122 with unit-cell dimensions of a = 123.8 Å and c = 458.5 Å (Table 2.1). COOT and PHENIX programs were used for model building and refinement (Afonine et al., 2012; Emsley and Cowtan, 2004). Statistical information regarding data collection and processing is presented in Table 2.1. Structural analysis was performed using coot, PyMOL, UCSF Chimera, GETAREA server.

Table 2.1. X-ray diffraction and refinement statistics

	Lamin S143F (residues 1-300)
Data collection	
Beamline	Pohang Accelerator Laboratory Beamline 5C
Wavelength (Å)	0.9794
Space group	I4122
Cell dimensions	
a, b, c (Å)	123.8, 123.8, 458.5
α, β, γ (°)	90, 90, 90
Resolution (Å)	48.1-3.7 (3.76-3.70)*
No. of reflections	18666
Rpim	0.02 (0.19)*
I/σI	19.2 (2.4)*
Completeness (%)	94.7 (80.5)*
Redundancy	9.2 (2.6)*
Refinement	
Resolution (Å)	48.1-3.7 (3.76-3.70)*
No. reflections	16492
Rwork/Rfree	0.287/0.304
Total no. of atoms	3271
No. ligands	0
No. water molecules	0
Wilson B-factor (Å 2)	11.1

RMS deviations	
Bond lengths (Å)	0.003
Bond angles (°)	0.563
Ramachandran plot	
Favoured (%)	99.25
Allowed (%)	0.25
Outliers (%)	0.0
PDB ID	**7D9N**

* Values in parentheses are for the highest resolution shell.

** Rp.i.m. = Σhkl (1/(n-1))1/2 Σi|Ii(hkl) − [I(hkl)]|/ΣhklΣiIi(hkl). Rpim is the precision-indicating (multiplicity-weighted) Rmerge.

***Rfree calculated for a random set of 9.9% of reflections not used in the refinement.

2.2.4. Pull-down assays

***This experiment was performed by Ph. D. Jinsook Ahn.**

A pull-down assay was conducted using a hexaHis-tagged lamin fragment (residues 250-400) immobilized on Ni-NTA resin as bait. The hexaHis-tagged cleaved lamin proteins as prey were incubated on His-tagged lamin immobilized resin pre-equilibrated in 20 mM Tris-HCl (pH 8.0) buffer containing 150 mM NaCl (or 50 mM NaCl) at room temperature for 30 min. After washing with buffer containing 20 mM Tris-HCl (pH 8.0), 150 mM NaCl, and 20 mM imidazole, the fractions were analyzed using SDS-PAGE.

2.3. Results

2.3.1. The overall structure of the lamin S143F mutant protein

The S143F mutant lamin A/C fragment (residues 1-300, referred to as the lamin 300 fragment) was over-produced in an E. coli expression system. The mutant lamin protein behaved as a dimer similar to the wild-type lamin 300 fragment as observed in previous reports (Ahn et al., 2019b); (Figure 2.1). The crystal structure was determined at 3.7 Å resolution by molecular replacement using half pieces of the wild-type lamin 300 fragment structure (PDB code: 6JLB) (Ahn et al., 2019b). The asymmetric unit contained one coiled-coil dimer, where the subdomains coil 1a, L1, coil 1b, and L12 regions were well ordered (residues 29-229 in one chain and residues 31-229 in the other chain) (Figure 2.2).

The coiled-coil dimer of the S143F mutant lamin showed elongated alpha-helix bending at linker L1 between coil 1a and coil 1b (Figure 2.2). Superposition of the S143F mutant and A:B or C:D coiled-coil dimers of the wild-type lamin structures have a root-mean-square deviation (RMSD) of 2.3 or 4.2 Å, respectively. A comparison to the wild-type lamin coiled-coil dimer structures showed that the bending directions of coil 1a are different with kinks at linker L1, reflecting conformational fluctuations of coil 1a and linker L1 with respect to coil 1b (Figure 2.1). The mutated Phe143 is at the ‘c’ position of the heptad repeat in coil 1b, orientating to the outside of the coiled-coil structure; thus, the mutation did not result in a substantial change in the coiled-coil structure of coil 1b (Figure 2.3).

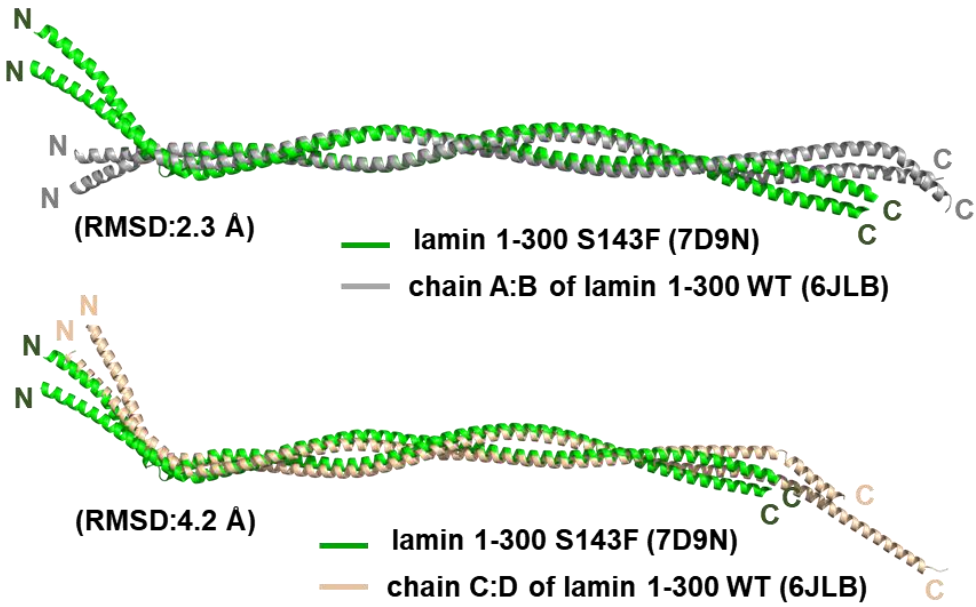

Figure 2.1. Structural superposition between the coiled-coil dimers of the wild-type and S143F mutant lamin 300

Structural superposition between the coiled-coil dimers of the wild-type (PDB ID: 6JLB, chain A:B; grey, chain C:D; wheat) and the S143F mutant lamin 300 fragments (this study; green).

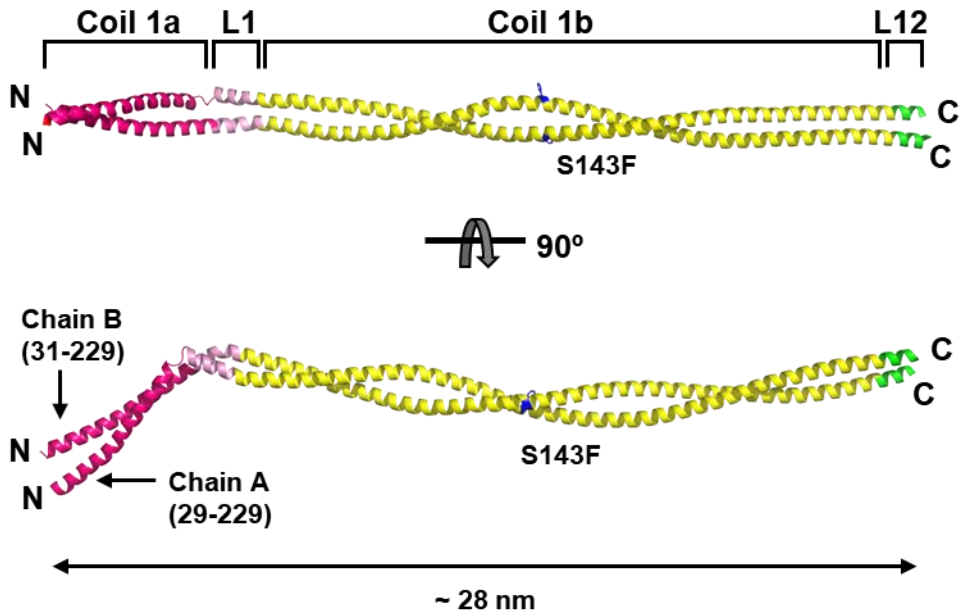

Figure 2.2. Crystal structure of the S143F mutant lamin 300 fragments (residues 1−300)

The asymmetric unit structure of the S143F mutant lamin fragment consists of two chains in a parallel coiled-coil arrangement. The ordered residues and the length of the coiled-coil dimer are indicated. Coil 1a is in pink, linkers L1 is in bright pink, coil 1b is in yellow, and L12 is in green. The Phe143 residues are colored blue in stick representation.

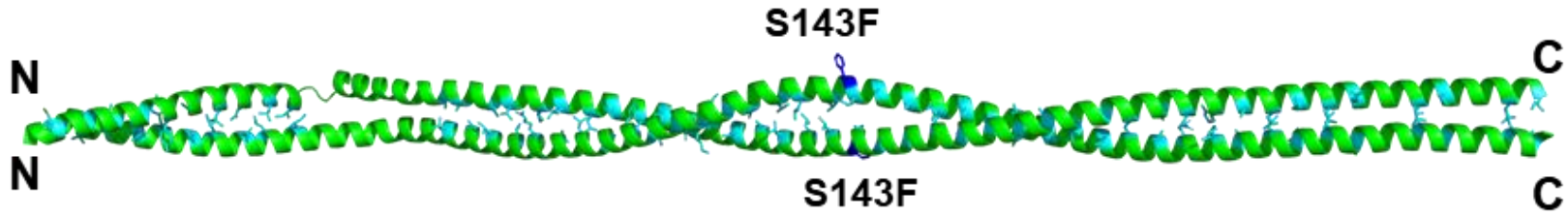

Figure 2.3. The inter-helical hydrophobic residues of lamin A 1-300 S143F

The heptad repeat's inter-helical hydrophobic residues are shown as cyan stick representations at the a and d positions. The Phe143 residues at the c position of the heptad repeat are in the magenta stick representations.

2.3.2. The S143F mutation does not change the interactions to make the linear filament

The crystallographic 2-fold symmetry built the A11 tetramer showing the antiparallel arrangement of the two dimers by overlapping the coil 1b region (Figure 2.4). Furthermore, the S143F mutant lamin does not interfere with the A11 interaction in forming the linear filament since the A11 tetrameric structures between the S143F and wild-type lamin A/C were similar overall with RMSD of 3.9 Å (Figure 2.5)

The A11 tetramers further assemble to elongate the filament via the so-called A22 interaction, representing the antiparallel arrangement between the entire coil 2 regions, including the coil 1a part. The direct and robust interaction between the insertion of the C-terminal region of coil 2 into the coil 1a region of the lamin 300 fragment was the key binding for the A22 interaction (Ahn et al., 2019b). Thus, to determine the mutational effect of S143F in terms of the A22 interaction, performing the pull-down assay that probed the A22 interaction using the C-terminal fragment of coil 2 (residues 250-400; called lamin 2C fragment) with the wild-type or S143F mutant lamin 300 fragments. In a previous study, the A22 interaction between the lamin 300 fragment and the C-terminal fragment of coil 2 shows strong at a relatively low NaCl concentration of 50 mM and weak binding at a relatively high NaCl concentration of 150 mM (Ahn et al., 2019b). Although the S143F mutation has occurred, the A22 interaction is shown equally as a wild-type (Figure 2.6). This finding was not surprising because Ser143 is not involved in the A22 binding interaction in the lamin 300 fragments.

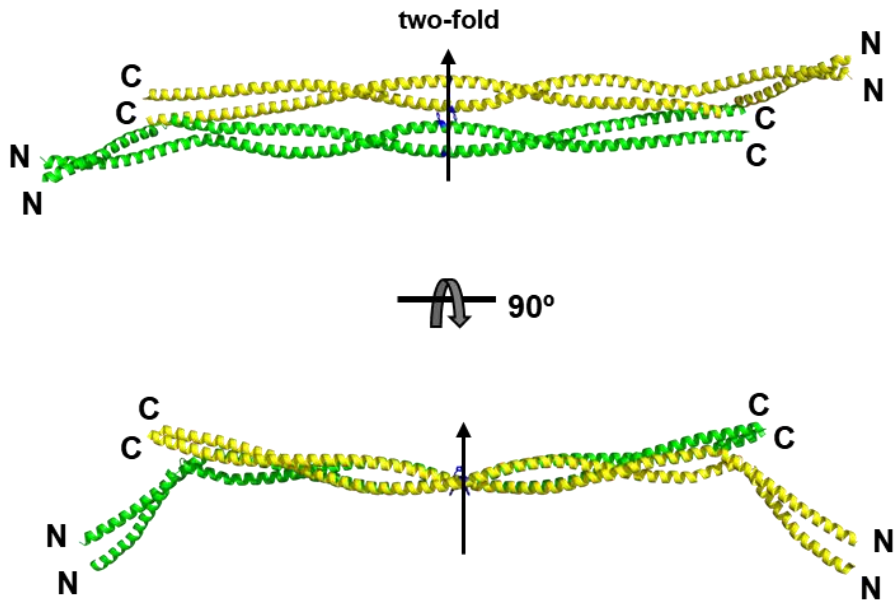

Figure 2. 4. The tetrameric unit of the S143F mutant lamin 300 fragments

The A11 tetramer structure was generated by applying crystallographic twofold symmetry to the asymmetric unit. The top and side views of the tetramer, consisting of two antiparallel coiled-coil dimers, are colored separately. A black arrow represents the twofold symmetry axis. The Phe143 residues are colored blue in stick representation.

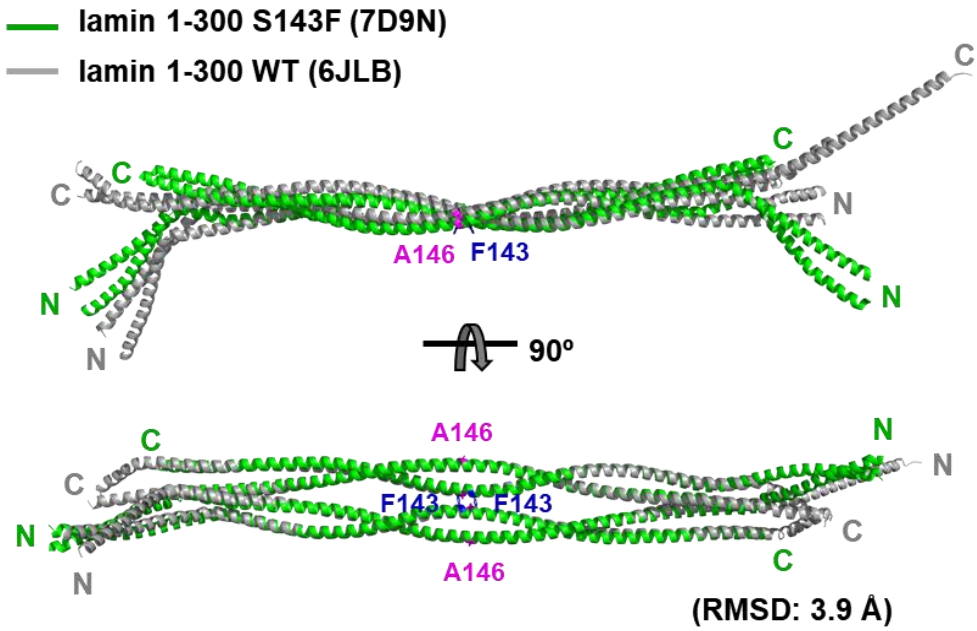

Figure 2. 5. The tetrameric structures of the wild-type and S143F mutant lamin 300 fragments

The A11 tetramers of the wild-type (PDB ID: 6JLB; grey) and S143F (PDB ID: 7D9N; green) lamin 300 fragments. The Ala146 residues are highlighted in magenta and represented by sticks.

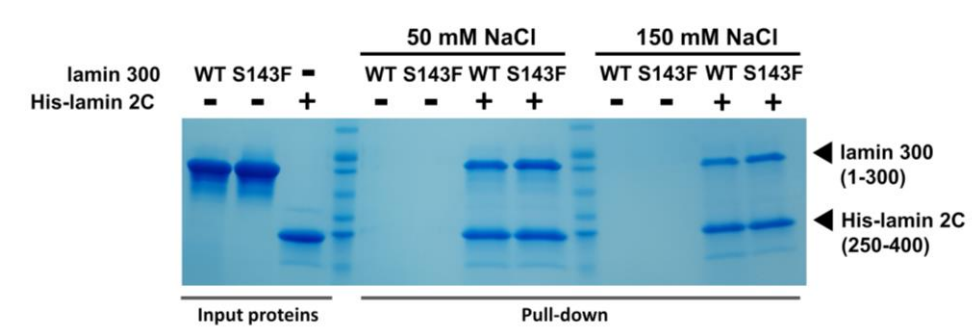

Figure 2. 6. Effects of the S143F mutation on the A11 and A22 interactions

***Ph. D. Jinsook-Ahn performed this assay.**

SDS-polyacrylamide gel showing the direct binding between lamin 300 and lamin 2 C fragment. The binding between the lamin 300 fragment (WT and S143F) and the hexaHis-tagged lamin fragment (His-lamin 2 C fragment; residues 250−400) was analyzed by pull-down experiments using Ni-NTA resin. The tagless lamin 300 fragments were incubated on the empty resin (−) or hexaHis-tagged protein-bound resin. Then, the resins were pre-equilibrated and washed with 20 mM Tris-HCl (pH 8.0) buffer containing 20 mM imidazole and 50 mM or 150 mM NaCl for pull-down, followed by SDS−PAGE analysis.

2.3.3. Phe143-mediated x-shaped interaction between the A11 tetramers

Two A11 tetramers directly interacted in the crystal since significant protein-protein interactions might be observed under highly condensed conditions in the crystal (Figure 2.7). Notably, the crystal structure of the S143F mutant lamin showed the x-shaped interaction between the two tetrameric units around Ala146 at the central residue of the tetramer (Figure 2.5). This x-shaped interaction between the A11 tetramers was not observed in the wild-type structure of the same lamin 300 fragment (Ahn, Jo et al. 2019). Notably, the mutated Phe143 residues were clustered on the surface of an x-shaped structure with the surface-exposed leucine residues Leu 137, Leu140, Leu141, Leu148, and Leu152 (Figure 2.7). Since the leucine residues were sandwiched between the A11 tetramer, the hydrophobic residues were four times more populated.

The surface hydrophobicity of the x-shaped region (residues 119-171) between the A11 tetramers was calculated using the Protein-Sol server (Hebditch and Warwicker, 2019). The S143F mutant protein exhibited maximum hydrophobicity at the x-shaped region around the Phe143 residue (3.94; corresponding to the hydrophobic association between heavy and light chains in the Fab domain). However, the corresponding x-shaped region of the wild-type protein was less hydrophobic than the peripheral region (2.66 at the peripheral region; Figure 2.8).

Thus, it might be reasonable that the mutated Phe143 residues were critical in triggering the x-shaped interaction between the A11 tetramers. Furthermore, the structure suggested that Phe143 exceeds the threshold to make the x-shaped

interaction by adding hydrophobicity to the binding interface in the center of the existing hydrophobic Leu residues on that tetramer.

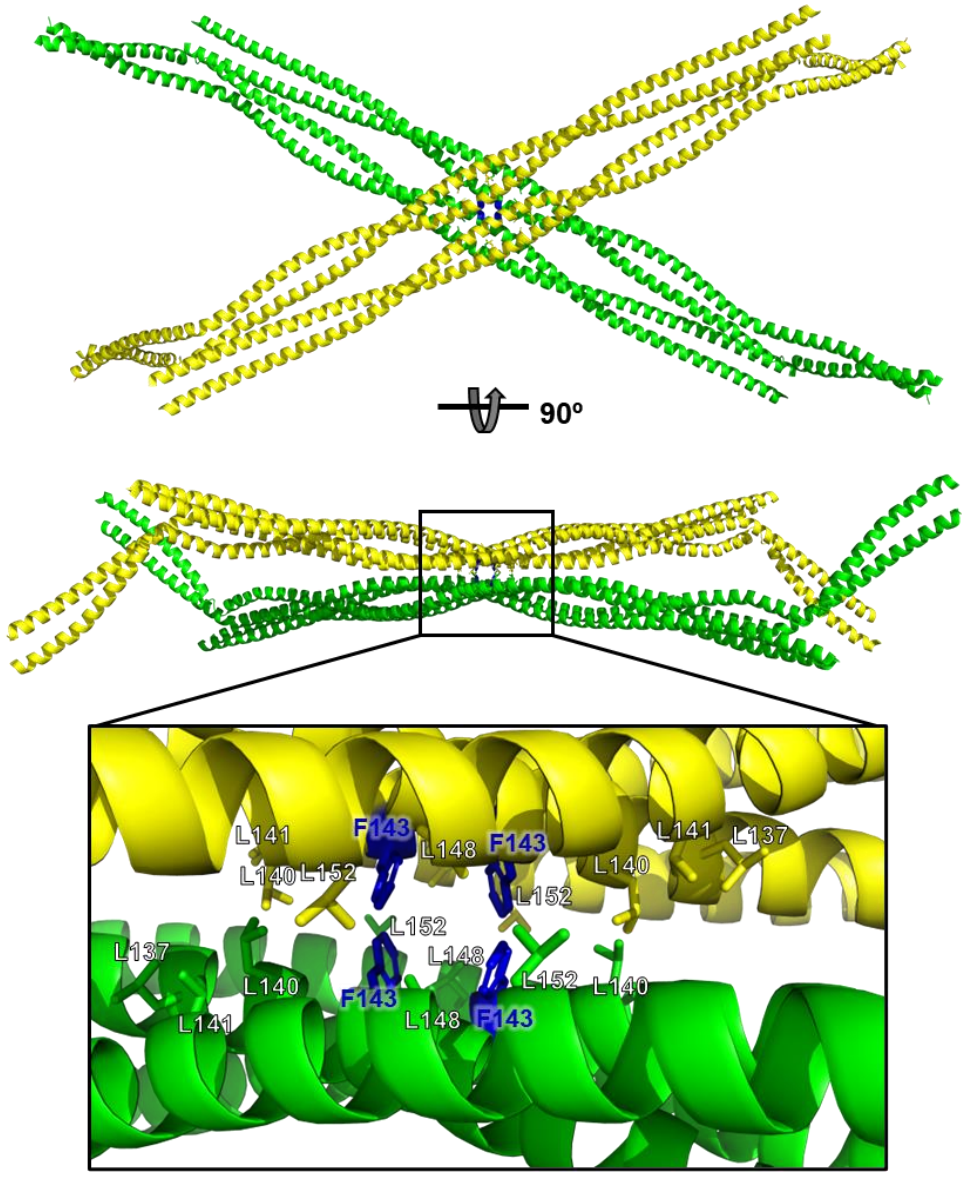
90°
L141
F143
L148
F143
L141
L137
L140
L152
L140
L152
L152
L137
L148
L140
L152
L140
F143
L141
L148
F143

Figure 2. 7. The X-shaped interaction between the two A11 tetramers of the S143F mutant lamin fragment in the crystals

The top and side views of the X-shaped interaction between the two A11 tetramers were generated by crystal packing interactions. The Phe143 residues are presented in the blue stick representations. The hydrophobic residues on the contact region for the X-shaped interaction between the two tetramers are shown in stick representations in the bottom panel.

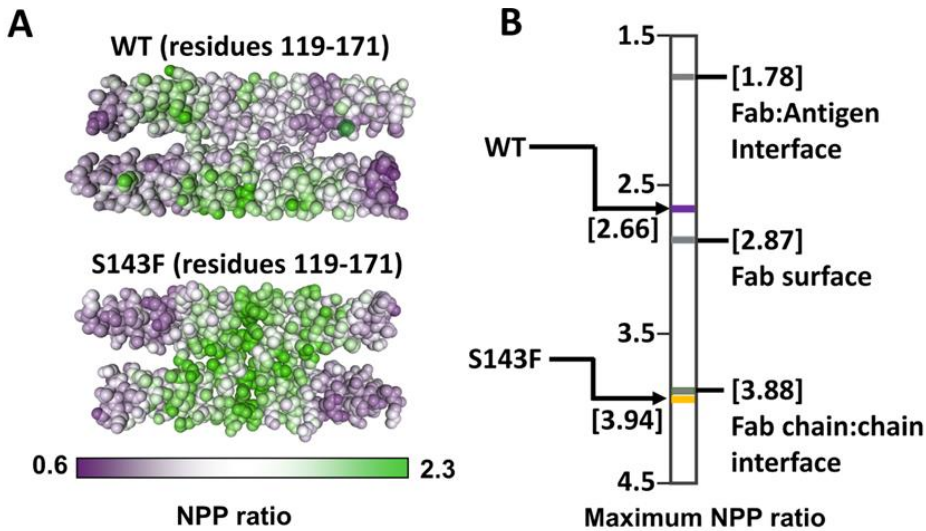

Figure 2. 8. Calculation of the surface hydrophobicity around the X-shaped contacting region (residues 119–171) of the wild-type and S143F mutant lamin A/C

***This analysis was conducted by Ph. D. Jinsook Ahn.**

A. Residues 119−171 were used to calculate the surface hydrophobicities of the wild-type and S143F mutant lamins. The values of the local nonpolar to polar ratio (NPP) are represented on the surfaces of the lamin proteins, color-coded from low NPP ratio (purple) to high NPP ratio (green). **B.** The maximum NPP values of the X-shaped contacting region on the lamin were calculated using the Protein-Sol server30. The standard maximum NPP values are displayed on the bar. The lamin S143F mutant has a higher surface hydrophobicity than the surfaces between the heavy and light chains of antibody Fab (Fab chain:chain interface).

2.3.4. Synergistic aggregation of the S149C mutation near Phe143 in the cell

The research group I belong to next investigated the effects of the S143F mutations based on the full-length lamin protein in the filament forms in the cells. The ectopic expression of the S143F mutant lamin A/C in HT1080 cells created the irregular aggregation of lamin A/C near the nuclear envelopes, as observed in previous reports (Figure 2.9) (Bercht Pfleghaar et al., 2015; Shimi et al., 2010). Ser 149 was noted near Phe143 on the surface of the x-shaped structure (Figure 2.7). Although the S143F mutant structure has a limited resolution to place the side chains accurately, the electron density map showed that the Ser149 residues are close enough to form a disulfide bridge between adjacent chains (Figure 2.10). Ser149 residue was changed to cysteine to form the site-specific disulfide bond, resulting in an x-shaped interaction similar to the S143F mutation (Figure 2.9). When lamin A/C harboring the mutations of S143F and S149C was transfected into the cells, the cells showed more severe nuclear deformation than both single-mutant lamins. This result suggests that the surface containing the Ser143 and Ser149 residues may be the platform to aggregate the full-length lamin A/C in the cell when it amplifies between adjacent lamin filaments.

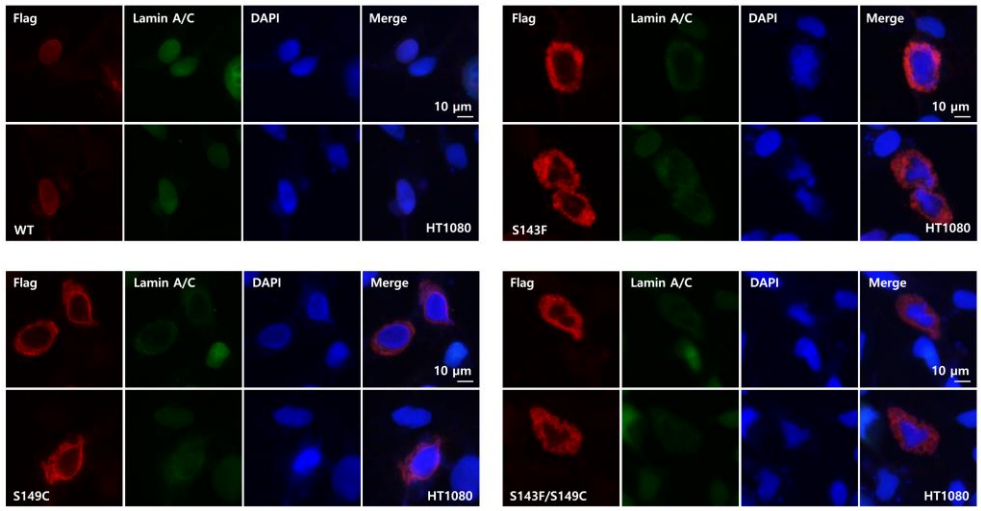

Figure 2. 9. Nuclear shapes and distribution of wild-type and S143F lamin A in HT1080 cells

***This experiment was conducted by Bum-Jun Park's lab.**

Immunofluorescence assays were performed to visualize the nuclear morphology after transfection the vector overexpressing wild-type or S143F Flag-tagged lamin A into HT1080 cells. For visualization of the nuclear membrane, cells were stained with an anti-Flag antibody for Flag-tagged lamin A (red), an anti-lamin A/C antibody for total lamin A/C (green), and DAPI for DNA (blue). The merged images of lamin A/C and DNA are displayed on the right (merge). Scale bar: 10 μm.

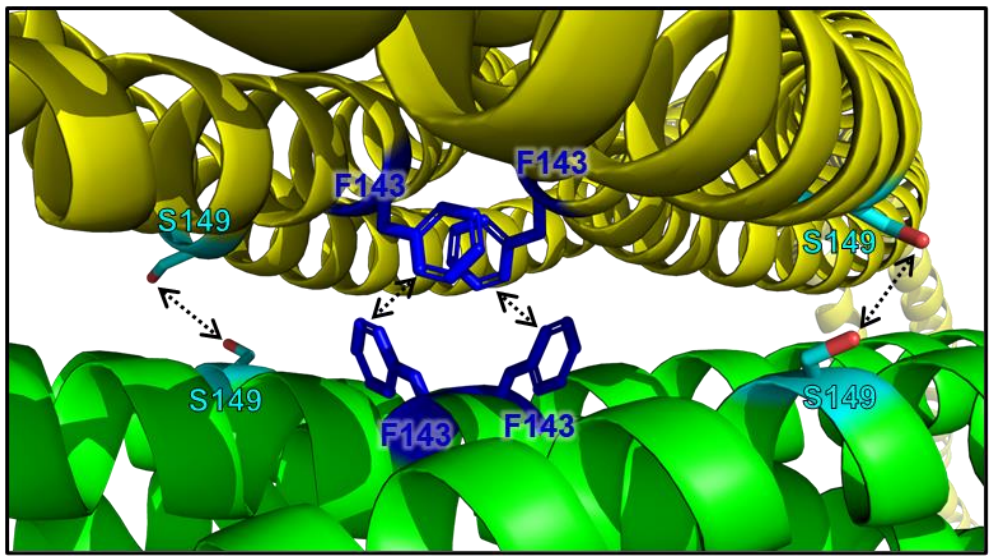

Figure 2. 10. The positions of Ser149 and Phe143 in the crossing-over structures between the two A11 tetramers

The positions of Ser149 and Phe143 in the X-shaped interaction between the two A11 tetramers. The Phe143 and Ser149 residues are depicted in the blue or cyan stick representations, respectively. Dotted lines indicate the shortest distances between the Phe143 residues or Ser149 residues.

2.4. Discussion

The currently prevailing model for HGPS has suggested that nuclear deformation results from the unprocessed farnesyl group of the altered C-terminal end of progerin (Gordon et al., 2014; Puttaraju et al., 2021). However, the S143F mutant lamin A/C also produced a deformed nuclear envelope structure even though the mutant lamin A/C does not contain the farnesyl group. Therefore, additional or other molecular mechanisms may exist in the nuclear deformation process caused by the progeroid syndrome. This study confirmed that the S143F mutation did not affect the A11 and eA22 interactions, which are the main forces for the linear filaments. Furthermore, these results indicate that the S143F mutation did not interfere with the 3.5-nm-thick linear filaments in the cell.

How could the S143F mutation cause local aggregation of lamin filaments around the nuclear cell membrane with nuclear deformation, as observed in progeroid syndrome cells? An expanded understanding is needed to answer the question of the lamin structure from the linear filaments to the x-shaped interaction between the linear filaments. This crystal structure of the S143F mutant lamin showed new molecular contacts around the substituted Phe143 residues, strengthening the x-shaped interaction between the A11 tetramers or the linear lamin filaments. It was noted that the aberrant x-shaped interaction between the filaments could ruin the 3-D meshwork structure of the nuclear lamin filament network.

The x-shaped interaction between the lamin filaments is critical in understanding the S143F mutational effect, even though the individual interactions

might not be strict. Phe143-containing hydrophobic surfaces present every A11 tetramer along the filament axis in the molecular model for the linear lamin filament (Figure 2.11) (Ahn et al., 2019b). This regular repeatability of the hydrophobic surfaces would result in positive cooperativity in the x-shaped interaction between the filaments (Figure 2.11). If two linear filaments have x-shaped interaction on the surface patch, the x-shaped interaction would be transient since only one contacting site exists between the two filaments (Figure 2.11i and ii). However, if four filaments are involved, every filament would make two contact sites, mutually enhancing the x-shaped interaction between the filaments (Figures 2.11iii and iv). Thus, once x-shaped interaction occurs at a region of the nuclear lamina, it would be generated gradually on the linear lamin filaments in a positive feedback manner (Figures 2.11i-v). The localized lamin deposition produced by the regularly repeated x-shaped interaction between the filaments would provide uneven rigidity on the nuclear lamina. The uneven rigidity might be the molecular reason for the blebbing or local aggregates of the lamin filaments in nuclear envelopes (Figure 2.11vi).

Aberrant inter-filament interactions are proposed as a common molecular cause between the S143F mutant lamin and progerin in progeroid syndrome. Progerin exhibited an aberrant interaction between the altered C-terminal end and the Ig-like domain of progerin or wild-type lamin A/C. Both existed regularly and repeatedly in the filaments (Ahn et al., 2021b; Kang et al., 2021; Lee et al., 2016). Since the C-terminal alteration at progerin is unlikely to interfere with linear filament formation, the aberrant interaction of progerin would cause crossing-over-like interactions between the filaments. Since both cases are formed between the

filaments that contain the regular and repeated binding sites, the interactions would be amplified in a positive-feedback manner, resulting in the local aggregation of the lamin filaments, which is the hallmark of progeroid syndromes. Recently, the molecular contacts using the chemical crosslinkers are accumulating in the lamin assembly (Ahn et al., 2019b; Makarov et al., 2019), in which the interactions were only applied to the linear filament formation. Some of the interactions probably contained the molecular contacts between the filaments during the meshwork formation.

In this study, a mechanism was proposed that local aggregation is strengthened when x-shaped interactions are amplified between adjacent lamin filaments during the formation of the 3-D meshwork. These findings suggest that abnormal 3-D meshwork formation may be responsible for the local aggregation of linear lamin filaments, leading to the deformation of the nuclear shapes. Further, “strengthened molecular interactions between the linear lamin filaments” presented a common mechanism to explain aging-related nuclear deformation.

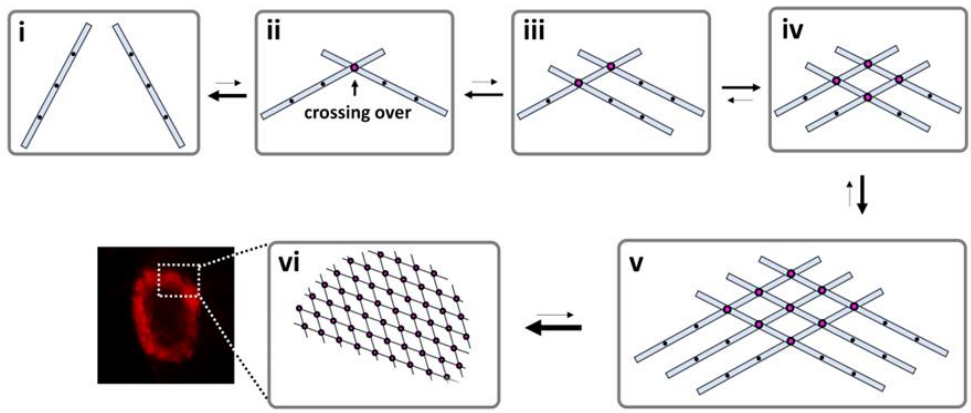

Figure 2. 11. The proposed mechanism for the aggregation of lamin filaments by the S143F mutation

A hypothetical mechanism is proposed to explain the mutual amplification of Phe143-triggered hydrophobic interactions. The two linear filaments form the reversible X-shaped interaction on the Phe143 sites (magenta circle) at low affinity **(i, ii)**. Another linear filament is joined to the existing filaments at a similar affinity on the Phe143 site near the preoccupying site, resulting in similar binding sites for recruiting the other lamin filaments **(iii)**. Finally, the fourth filament is bound to the two Phe143 sites simultaneously, resulting in a mutual binding platform at a higher binding affinity **(iv)**. The equilibrium is increasingly shifted to the association as more filaments are recruited. All linear filaments make contacts on more Phe143 sites **(v)**, resulting in local aggregation on the nuclear membrane **(vi)**.

Chapter 3.

Cyclin-dependent Kinase 1 depolymerizes nuclear lamin filaments by disrupting the head-to-tail interaction of the lamin central rod domain.

Published in JBC

Jeong, S., Ahn, J., Jo, I., Kang, S. M., Park, B. J., Cho, H. S., ... & Ha, N. C. (2022). Cyclin-dependent kinase 1 depolymerizes nuclear lamin filaments by disrupting the head-to-tail interaction of the lamin central rod domain. Journal of Biological Chemistry, 298(9).

3.1. Introduction

Intermediate filaments (IFs) form a robust protein network in the cytoplasm of most cells to provide mechanical strength to the cells (Herrmann and Aebi, 2004; 2016). All IFs share a typical structural organization, although they are substantially diverse in size and amino acid sequence. IFs can be divided into cytosolic and nuclear families by the features of the primary structures. All IFs consist of the central α-helical rod domains, N-terminal head, and C-terminal tail regions (Aebi et al., 1988; Fuchs and Weber, 1994; Herrmann et al., 2003). The central α-helical rod domains are responsible for forming the parallel coiled-coil dimer due to its characteristic periodicities in the sequence. The central α-helical domains are divided into several subdomains: coil 1a, linker L1, coil 1b, linker L12, and coil 2. The periodicities in the coil 2 region are different in the regions: hendecad repeats (residues 241-277), heptad repeats (278-319), stutter (residues 320-330), and heptad repeats (residues 331-385) (Figure 3.1) (Ahn et al., 2019b; Chernyatina et al., 2015; Parry, 2006).

The nuclear IF lamins form a robust meshwork structure near the inner nuclear membrane inside the nucleus, primarily maintaining the nuclear envelope structure (Liu and Ikegami, 2020; Prokocimer et al., 2009; Turgay et al., 2017; Xie et al., 2016). The nuclear IF lamin A/C is expressed in differentiated cells, unlike lamin B1 and B2, which are ubiquitously expressed in eukaryotic cells (Dittmer and Misteli, 2011; Goldman et al., 2002). In situ cryo-EM images of the lamin A/C filaments have revealed that the thinner 3.5-nm-thick filament structure is distinct from the cytosolic IFs that exhibit the typical 10-nm-thick filament (Turgay et al., 2017). Four types of dimer-to-dimer interaction modes (A11, A22, A12, and ACN)

have been observed in IFs when forming the mature filament (Chernyatina et al., 2015; Eldirany et al., 2021a; Steinert et al., 1993). The lamin filament model was proposed using three types of interaction modes (A11, A22, and ACN) based on the cryo-ET and chemical cross-linking data (Ahn et al., 2019b; Makarov et al., 2019; Stalmans et al., 2020; Vermeire et al., 2021). They further proposed that four or more units of the 3.5-nm thick filaments are laterally assembled into 10-nm-thick filaments of cytosolic IFs in the A12 interaction mode.

The structure of the long lamin A/C fragment (residues 1-300) has been shown to have an antiparallel arrangement of two parallel coiled-coil dimers at 3.2 Å resolution (Ahn et al., 2019b). This antiparallel arrangement of lamins was designated as the 'A11' interaction, previously named due to the antiparallel interaction between the coil 1b regions from the adjacent coiled-coil dimers (Herrmann and Aebi, 2004; Vermeire et al., 2021). The A11 tetramers, formed by the A11 interaction, are further joined to elongate the linear filament by another interaction mode, A22, representing an antiparallel arrangement between the coil 2 regions (Eldirany et al., 2021a; Lilina et al., 2020). The interaction mode, called ACN, represents a head-to-tail arrangement between coil 1a and the C-terminal region of coil 2. The sophisticated cross-linking mass analysis and modeling studies further suggested that the A22 and ACN interaction modes consequently indicate the same arrangement of the A11 tetramers. The A22 or ACN binding modes include not only the interaction between the coil 2 (referred to as A22 interaction) but also the coil 1a and the C-terminal region of coil 2 (referred to as ACN interaction) are formed (Makarov et al., 2019; Steinert et al., 1993; Vermeire et al., 2021).

The disappearance of the nuclear envelope is the hallmark of mitosis in eukaryotic cells (Dessev et al., 1990; Gerace and Blobel, 1980; McKeon, 1991). A critical feature of nuclear lamins is cell cycle-dependent polymerization and depolymerization, which determines the morphology of the nuclear envelope. To date, 92 phosphorylation sites that mainly concentrate in the head and the tail domain of lamin A/C have been identified in lamin A/C throughout the cell cycle (Liu and Ikegami, 2020; Omary et al., 2006). The activated CDK1/cyclin B complex at the onset of mitosis phosphorylates the lamin filaments, leading to the depolymerization of the filaments and a breakdown of the nuclear envelope (Heald and McKeon, 1990; Peter et al., 1990; Ward and Kirschner, 1990). Phosphorylation at Thr19 and Ser22 in the lamin N-terminal region by the CDK1/cyclin B complex is known as the critical step for cell cycle-dependent disassembly of the lamin filamentous structure (Heald and McKeon, 1990; Kochin et al., 2014). The mutation at Ser22 to Leu was associated with dilated cardiomyopathy (Pethig et al., 2005). However, its phosphorylation-dependent lamin disassembly mechanism is poorly understood at the molecular level. In this study, the mechanism was investigated by which phosphorylation acts on the molecular interactions in the 3.5-nm-thick filament of lamin proteins.

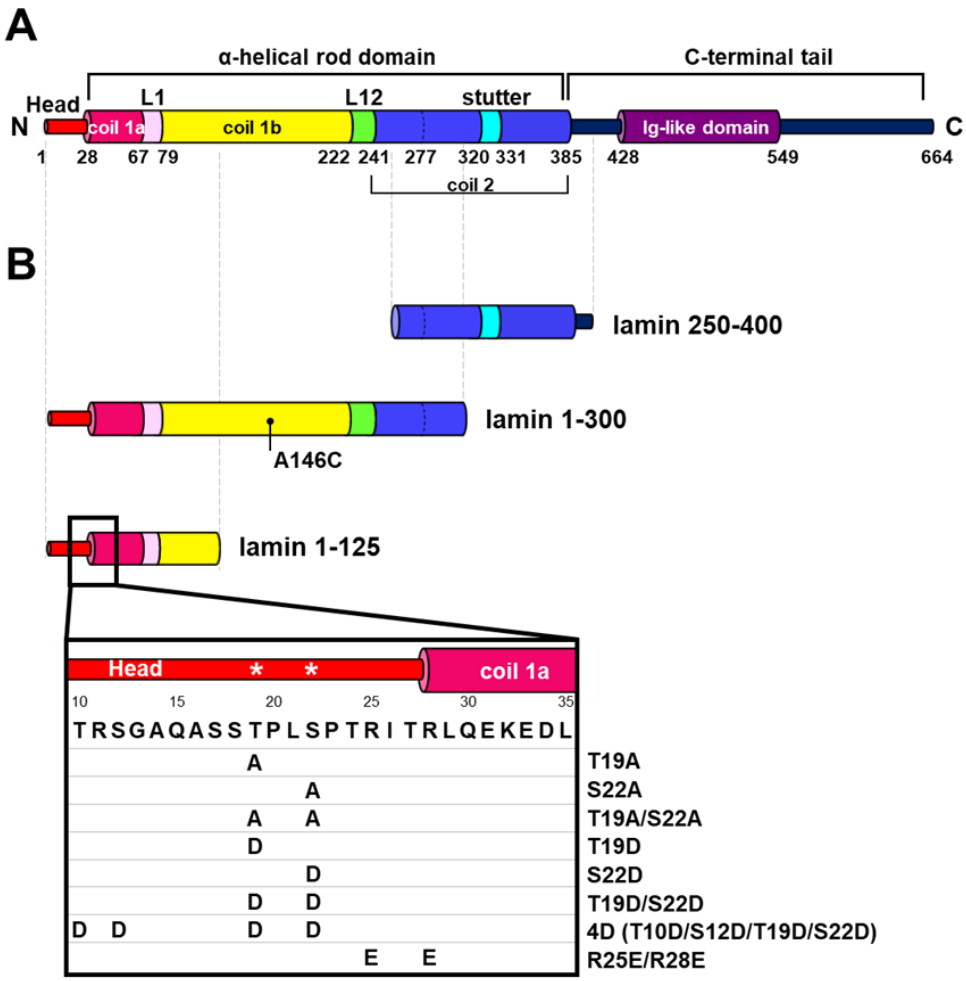
A
α-helical rod domain
C-terminal tail
Head
L1
L12
stutter
N
coil 1a
coil 1b
Ig-like domain
C
1
28
67
79
222
241
277
320
331
385
428
549
664
coil 2
B
lamin 250-400
lamin 1-300
A146C
lamin 1-125
Head
coil 1a
10
15
20
25
30
35
T R S G A Q A S S T P L S P T R I T R L Q E K E D L
T19A
S22A
T19A/S22A
T19D
S22D
T19D/S22D
4D (T10D/S12D/T19D/S22D)
R25E/R28E

Figure 3. 1. The structural organization of lamin A/C and the lamin fragments used in this study

A. schematic diagram of the organization of lamin A/C, including the N-terminal head, the central α-helical rod, and the C-terminal tail domains. The subdomains coil 1a, linker L1, coil 1b, linker L12, coil 2, stutter, and coil 2 are labeled in the α-helical rod domain. The C-terminal tail contains the immunoglobulin (Ig)-like domain (violet). The unstructured regions are in thinner cylinders. **B.** the lamin fragments used in this study: lamin 250 to 400, lamin 1 to 300, and lamin 1 to 125 fragments. The amino acid sequence of residues 10 to 35 is shown in the enlarged images in the box. Asterisks indicate the CDK1 phosphorylation sites. The mutants used in this study are indicated in the corresponding positions. CDK1, cyclin-dependent kinase 1.

3.2. Materials and Methods

3.2.1. Expression and purification of proteins

Wild-type lamin 1-125 fragment (human lamin A/C, residues 1-125) and mutant forms (T19A, S22A, T19A/S22A, S22D, T19D/S22D, T10D/S12D/T19D/S22D, R25E/R28E) with an N-terminal hexaHis-tag were expressed in E. coli as previously described (Ahn et al., 2020). Human lamin A/C 250-400 (coil 2C-containing fragment in the main text) was expressed in E. coli as an N-terminal GST-fusion protein. Cells were cultured in a Terrific broth medium at 37 °C overnight, induced with 0.5 mM isopropyl β-D-1 thiogalactopyranoside (IPTG), and grown for another 6 hrs. After the cells were harvested, they were resuspended in lysis buffer (20 mM Tris-HCl pH 8.0, 150 mM NaCl, and 2 mM β-mercaptoethanol) and then disrupted using a French press (23 kpsi). The cell debris was removed by centrifugation, and the supernatant was loaded onto glutathione-agarose resin (GE Healthcare, USA), which was preincubated with a lysis buffer. The target protein was eluted with lysis buffer supplemented with 20 mM reduced GSH. For further purification, the target protein was loaded onto a HiTrap Q column (GE Healthcare, USA) and eluted with 300 mM NaCl. The purified proteins were desalted using a HiPrep 16/60 desalting column (GE Healthcare, USA) in 20 mM Tris-HCl (pH 7.5) and 50 mM NaCl.

The catalytic domain (residues 1-319) of the human CK1ε catalytic domain with the C-terminal hexaHis-tag was expressed in E. coli (Ha et al., 2004). The bacterial cells were cultured in a Luria-Bertani medium at 37 °C until an optical density at 600 nm (OD600) of 0.7, and the protein was expressed by

induction with 0.5 mM IPTG for 6 hrs. After the cells were harvested, they were resuspended in lysis buffer (20 mM Tris-HCl pH 7.5, 150 mM NaCl, and 2 mM β-mercaptoethanol) and then disrupted using a French press (23 kpsi) and cleared by centrifugation. The supernatant was loaded onto Ni-NTA resin (GE Healthcare, USA) was preincubated in a lysis buffer. CK1ε was eluted with lysis buffer supplemented with 250 mM imidazole and 0.5 mM EDTA (ethylene-diamine-tetraacetic acid). The eluted protein was loaded on a HiLoad 16/600 column (GE Healthcare, USA) with 20 mM Tris-HCl pH 7.5, 150 mM NaCl, 0.5 mM EDTA, and 2 mM β-mercaptoethanol. The recombinant GSK3β protein was obtained as outlined previously (Kim et al., 2018).

3.2.2. Phosphorylation of the lamin N-terminal fragment

One hundred micrograms of each lamin fragment were phosphorylated by 1 μg of the CDK1/cyclin B complex protein (#PV3292, Thermo Fisher, USA) or CK1ε or GSK3β for 2 hrs at 30 °C in 200 μl of 20 mM Tris-HCl, pH 7.5 buffer containing 50 mM NaCl, 20 mM MgCl2, 0.5 mM EDTA, 1 mM ATP, and 2 mM 1,4-dithiothreitol (DTT). The reaction was stopped by adding 10 μM flavopiridol (CDK1 inhibitor, Selleckchem, USA) to the reaction mixture.

3.2.3. GST pull-down assays

The phosphorylated or nonphosphorylated lamin N-terminal fragments (20 μM) and GST-fused coil 2C fragment (5 μM) were incubated in 300 μl of 20 mM Tris-HCl (pH 7.5) buffer containing 50 mM NaCl with GSH-agarose resin for one hr at room temperature. The resins were washed with 50 mM Tris-HCl (pH 7.5)

buffer containing 50 mM NaCl and eluted with buffer supplemented with 20 mM reduced GSH. The samples were analyzed by a 4-20% gradient SDS-polyacrylamide gel (Bio-Rad, USA) or a Phos-tag containing SDS-polyacrylamide gel (Wako, Japan).

3.2.4. Lamin coil 2-conjugated Sepharose pull-down assay

The GST-fused lamin coil 2C-containing fragment was conjugated with the resin using cyanogen bromide (CNBr)-activated Sepharose (GE Healthcare, USA), resulting in lamin coil 2-conjugated Sepharose. The lamin coil 2-conjugated Sepharose was washed with 20 mM Bis-Tris propane pH 7.5 buffer or 20 mM Bis-Tris propane pH 9.5 buffer. Each washing buffer contained 50 mM NaCl. The lamin 1-125 fragment (50 μg) was incubated with lamin coil 2-conjugated Sepharose for 1 hr at room temperature. The Sepharose resins were washed with washing buffer and loaded on SDS−PAGE gels (Bio-Rad, USA).

3.2.5. Circular dichroism (CD)

The purified wild-type and mutant lamin 1-125 fragments (1 mg/ml) were dialyzed against PBS. Then, the CD spectra were recorded by UV from 190 nm to 260 nm in the circular dichroism detector Chirascanplus (AppliedPhotophysics, UK). The protein secondary structure elements were analyzed using CDNN software (Circular Dichroism analysis using Neural Networks) (Bohm et al., 1992).

3.2.6. Lamin complex modeling

The N-terminal flexible head region structure was predicted by Alphafold 2 colab (Jumper et al., 2021) using the lamin sequence (residues 1-80). The parallel four-helix bundle structure of coil 1a (residues 28-67) and coil 2C (residues 327-385) was built by using a typical parallel four-helix bundle structure (protein data bank (PDB) code: 1G1J) as the structural template. The residues were changed into the sequences of coil 1a and coil 2C based on the sequence alignment by referring to the model of Stalman et al. (Stalmans et al., 2020). The N-terminal head region and parallel four-helix bundle structure were combined and refined by GalaxyRefineComplex (Heo et al., 2016).

3.3. Results

3.3.1. The phosphorylation of lamin by CDK1 inhibits the A22 interaction

To examine whether phosphorylation at the N-terminal fragments affects the A11 type interaction, I performed an in vitro binding assay using the lamin 1-300 fragment (residues 1−300) harboring the A146C mutation (Figure 3.1A) (Ahn et al., 2019b). The lamin 1-300 fragment contains the head region (residues 1-27) and the central rod domain, which forms A11 tetramers without the A22 interaction. The disulfide bond between two coiled-coil dimers would be created within the A11 tetramer since Ala146 is in the center of the A11 tetramer, as confirmed in the crystal structure (Ahn et al., 2019b). Thus, I monitored the propensity of the A11 interactions as the amount of the disulfide forms by utilizing the A11-tetramer-dependent disulfide bond formation of the A146C mutant protein (Ahn et al., 2019b).

The A146C mutant lamin 1-300 fragments were phosphorylated by the CDK1/cyclin B complex. To distinguish the phosphorylated bands, I used a Phos-tagTM containing sodium dodecyl sulfate-polyacrylamide gel electrophoresis (SDS-PAGE), in which the Phos-tag retarded the mobility of the phosphorylated proteins by the specific interaction with the phosphate group (Figure 3.2, (p)-lamin 1-300 in lanes 1 and 3) (Kinoshita et al., 2012). These results confirm that the CDK1/cyclin B complex phosphorylates the lamin 1-300 fragments. The amounts of the disulfide form of lamin 1-300 (A146C) under nonreducing conditions were identified to reflect the propensity of A11 tetramer formation. Similar amounts of

disulfide forms were observed between the nonphosphorylated and phosphorylated lamin proteins. These results indicate that the A11 interaction is not significantly affected by the phosphorylation of the N-terminal head region by the CDK1/cyclin B complex (Figure 3.2A, disulfide-bonded lamin 1-300 in lanes 5 and 6).

The experiment was performed to test whether phosphorylation by the CDK1/cyclin B complex affects the A22 or ACN-type interaction. To monitor and distinguish the ACN mode and A22 interactions, I used two lamin N-terminal fragments and one lamin C-terminal fragment. The lamin 1-125 (residues 1-125) and lamin 1-300 fragments were used for the lamin N-terminal fragment. For the C-terminal lamin fragment, I used a lamin 250-400 fragment (residues 250-400), which spans most of the entire coil 2 (residues 242-385) and a C-terminal flanking region (residues 386-400). The lamin 250-400 fragment contains the structural elements for ACN mode, consistent with the after-stutter region composed of the heptad repeat periodicity (residues 331-385, Figure 3.1A). Since the lamin 1-125 fragment does not contain the coil 2 region for the A22 type interaction, this fragment can detect only the ACN mode and not the A22 interaction. In contrast, the lamin 1-300 fragment could participate both in the A22 interaction and the ACN mode.

I first confirmed that both the lamin 1-125 and 1-300 fragments were phosphorylated well by the CDK1/cyclin B complex (the upshifted bands for the lamin 1-125 fragment in Figure 3.3A lanes 1and 3). In a glutathione-S-transferase (GST) pull-down assay to test the ACN and A22 interaction modes, phosphorylated lamin N-terminal 1-125 and 1-300 fragments were weaker bindings to GST-fused lamin C-terminal 250-400 fragment than the unphosphorylated lamin N-terminal

fragments. These observations showed that phosphorylation at the lamin N-terminal head region weakened the interaction with the lamin coil 2 region (Figure 3.3B right lanes 1 and 3). Since the phosphorylation of lamin influenced the interaction with the lamin 1-125 fragment that cannot participate in the A22 interaction, these findings further showed that phosphorylation is involved in the ACN interaction but not in the A22 interaction.

The lamin complex of the lamin 1-125 fragment and the lamin 250-400 fragment in glutathione (GSH)-coupled resin was prepared to test whether phosphorylation induces the dissociation of the complex in a reasonable time. Then, the lamin complex bound to the resin was incubated with the CDK1/cyclin B complex for two hours to allow the CDK1 enzyme to phosphorylate the lamin complex. As a result, the lamin complex was phosphorylated by the CDK1 enzyme as efficiently as the individual lamin fragment proteins. These results demonstrate that the CDK1 acts on the lamin complex to induce the dissociation of the lamin complex on a feasible time scale (Figure 3.4).

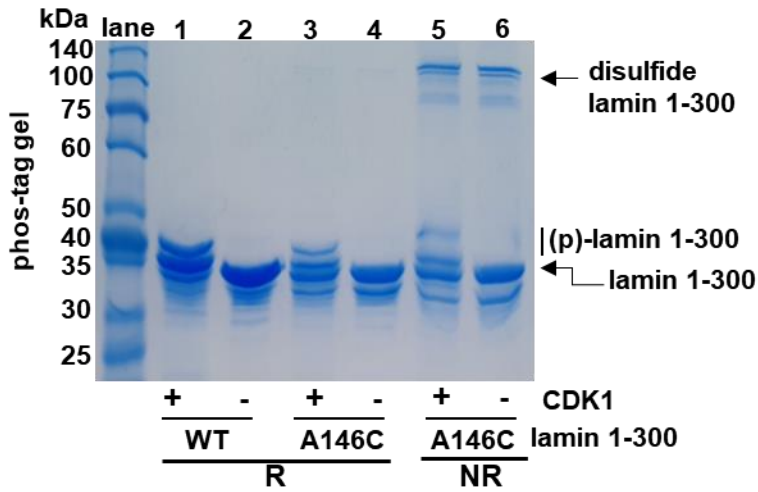

Figure 3. 2. The effects of CDK1–cyclin B1 activity on lamin proteins in the A11 interactions

There was monitored the A11 interaction by the phosphorylation of the lamin 1 to 300 fragment by the CDK1 complex. The WT and A146C mutant lamin 1 to 300 fragments were phosphorylated by the CDK1 complex and then analyzed by a Phos-tag–containing SDS-polyacrylamide gel using reducing loading dye (R) or nonreducing loading dye (NR). The phosphorylated lamin 1 to 300 ((p)-lamin 1 to 300) fragment moved slower than the unphosphorylated lamin 1 to 300 in the Phos-tag–containing gel. Noted that the disulfide-bonded lamin 1 to 300 fragment (disulfide lamin 1–300) formed regardless of the CDK1-mediated phosphorylation. GST, glutathione-S-transferase.

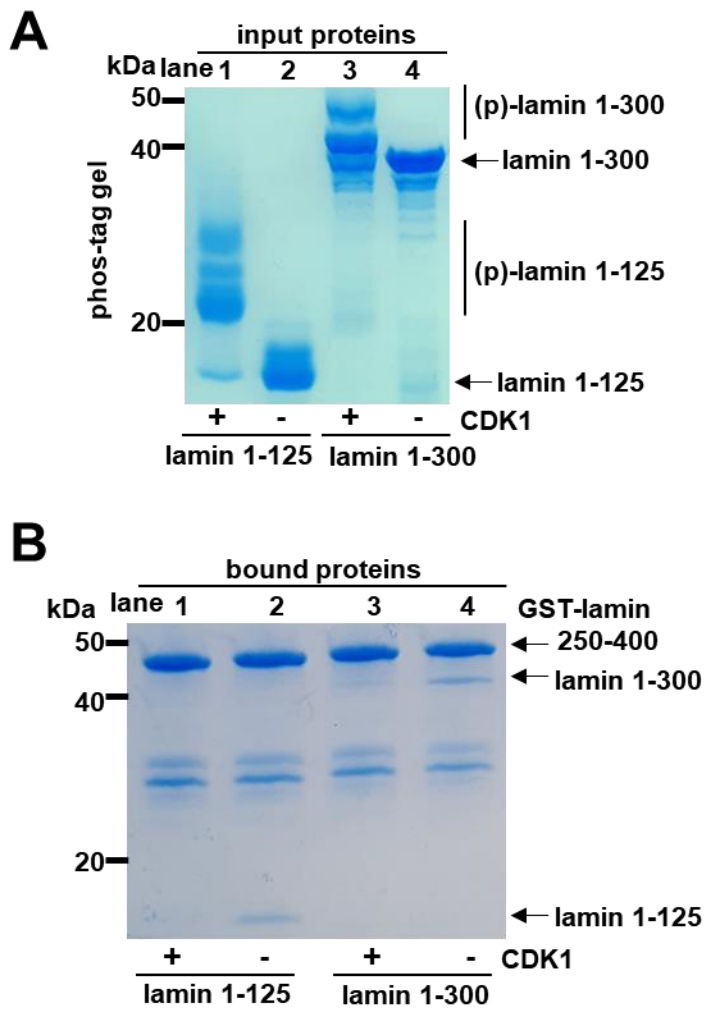

Figure 3. 3. The effects of CDK1–cyclin B1 activity on lamin proteins in the A22 interactions

A. Phosphorylation of lamin N-terminal fragments (lamin 1−125; lamin 1−300) by the CDK1 complex represents the Phos-tag-containing gel. **B.** The bound protein, which represents the results of ACN interaction, is on the right SDS-polyacrylamide gel. The standard size markers are in the left lane in each gel. CDK1, cyclin-dependent kinase 1; GST, glutathione-S-transferase.

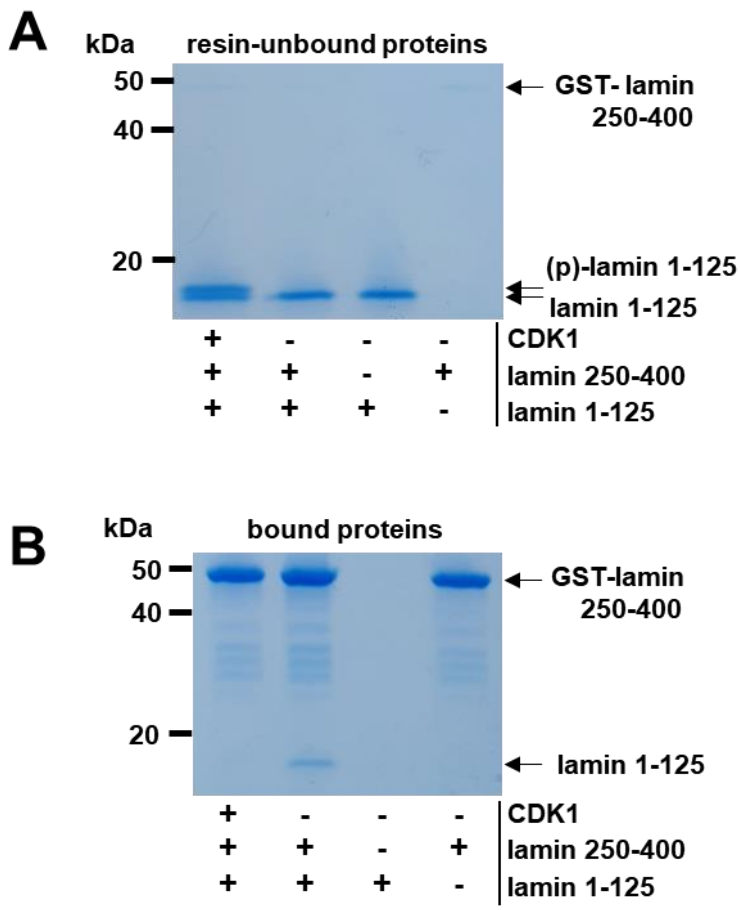

Figure 3. 4. Dissociation of the lamin complex by CDK–cyclin B activity

A. The resin of the lamin complex, consisting of lamin 1 to 125 and lamin 250 to 400 fragments, was incubated with the CDK1−cyclin B complex at room temperature. **B.** The resins were washed, and then the bound proteins were analyzed by SDS-PAGE. CDK1, cyclin-dependent kinase 1; GST, glutathione-S-transferase.

3.3.2. Phosphorylation of Thr19 and Ser22 inhibits the ACN mode

The Thr19 and Ser22 residues in the lamin N-terminal head region are the target sites of the CDK1/cyclin B complex in the depolymerization of lamin filaments during mitosis (Adhikari et al., 2012; Chen et al., 2013; Kochin et al., 2014). To determine which residues are more important in regulating the ACN mode dependent on CDK1 activity, single and double mutants were created at the lamin 1-125 fragment at Thr19 and Ser22: T19A, S22A, and T19A/S22A. The phosphorylation of the mutant lamin fragments by the CDK1 complex was assessed by mobility shifts on Phos-tag PAGE (Figure 3.5A). The double mutant T19A/S22A protein underwent a band shift, indicating the other CDK1 target sites in the lamin fragment containing residues 1 to 125.

The mutant lamin 1-125 fragments participated in the ACN mode as robustly as the wild-type fragment (Figure 3.5B, the right panel, Lanes 5-8), indicating that Thr19 and Ser22 are not involved in mediating the ACN interaction. However, when the lamin 1-125 fragments were phosphorylated by CDK1, the mutant lamin 1-125 fragments retained the ACN with the C-terminal fragment of lamin A/C coil 2, unlike the wild-type fragment (Figure 3.5B, the right panel, Lanes 1-4). Furthermore, when phosphorylated, the double mutant T19A/S22A protein showed a more evident effect than the single mutant proteins T19A and S22A. Thus, these findings suggest that phosphorylation at Thr19 and Ser22 in the lamin N-terminal region cumulatively contributes to the depolymerization of the lamin filaments. These results are consistent with the previous results for Thr19 and Ser22 in the cell cycle-dependent depolymerization of lamin filaments (Kochin et al., 2014).

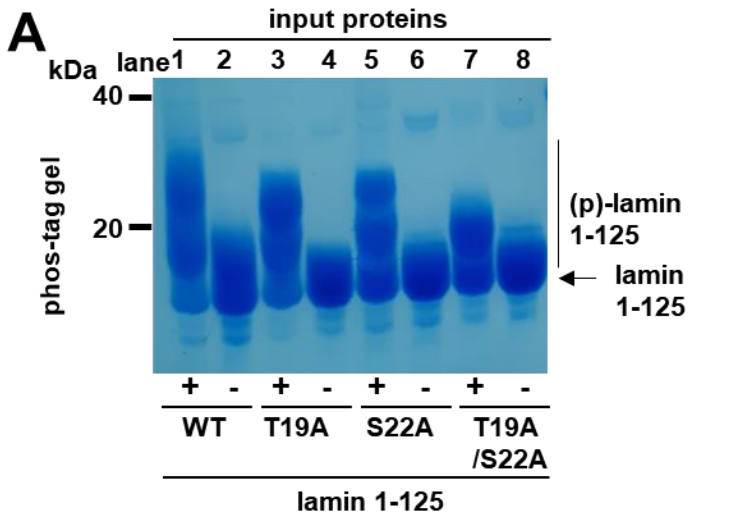
A
input proteins
kDa
lane 1 2 3 4 5 6 7 8
40
20
phos-tag gel
(p)-lamin
1-125
lamin
1-125
+ - + - + - + -
WT
T19A
S22A
T19A
/S22A
lamin 1-125

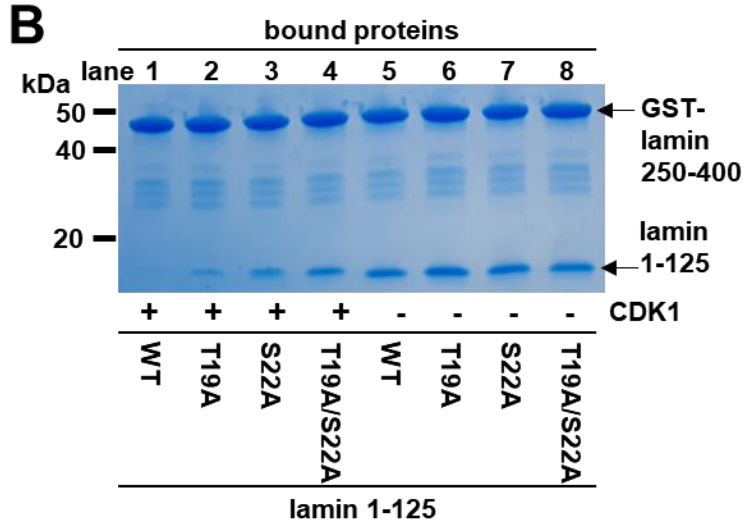
B
bound proteins
kDa
lane 1 2 3 4 5 6 7 8
50
40
20
GST-
lamin
250-400
lamin
1-125
+ + + + - - - - CDK1
WT
T19A
S22A
T19A/S22A
WT
T19A
S22A
T19A/S22A
lamin 1-125

Figure 3. 5. Phosphorylation of Thr19 and Ser22 and performing GST-pull down assay

A. The amount of phosphorylation of WT or mutant lamin 1 to 125 is exhibited by phos-tag PAGE. The lamin 125 fragments harboring the mutations T19A, S22A, and T19A/S22A were phosphorylated by treating the CDK1/cyclin B complex (0.5 μg/ml) for 2 hrs at room temperature. The phosphorylated protein bands ((p)-lamin 125; Lanes 1, 3, 5, and 7) are at slightly higher positions than the nonphosphorylated protein bands (Lanes 2, 4, 6, and 8). **B.** The amounts of the various mutant lamin 1 to 125 fragments bound to the GST-fused lamin 250 to 400 represent the ACN mode. CDK1, cyclin-dependent kinase 1; GST, glutathione-S-transferase.

3.3.3. The phosphorylation of lamin A/C/ does not affect the coiled-coil structure of coil 1a

Then, how does phosphorylation in the N-terminal head region abolish the ACN interaction? The phosphorylation effects on the propensity for coiled-coil formation were first investigated to answer this question (Figure 2.6). The coil 1a region was noted to be adjacent to the phosphorylation sites because the coiled-coil tendency of the coil 1a region was reversely correlated to the ACN interactions in the L59R mutant (Ahn et al., 2020; Kang et al., 2018).

Based on the circular dichotomy (CD) results with the refined laminate fragments, it was investigated whether the phosphorylation of the laminate 1-125 fragment affects the coil-coil propensity of the coil 1a region. This experiment used the phosphorylation-mimicking dual mutant T19D/S22D and quadruple mutant T10D/S12D/T19D/S22D (designated the 4D mutant in this study) instead of the phosphorylated lamin fragment. The dual and quadruple mutants were employed in this CD experiment because the phosphorylated protein samples could not be obtained enough for the CD analysis. Phosphorylation at Thr10 and Ser12 was observed in the cellular lamin proteins, although the responsible kinases were unknown. In addition, the 4D mutation completely abolished the ACN between lamin 1-125 and lamin 250-400 fragments, while the ACN interaction was partially retained in the T19D/S22D mutant (Figure 3.7). Although the dual and quadruple mutations did not completely mimic phosphorylation by the CDK1 complex, these findings suggest that the charge introduction is essential in inhibiting the ACN mode without changing the coiled-coil propensity of the lamin 1-125 fragments (Figure 3.8).

The genetic L59R mutation significantly weakened the helical propensity in the lamin 1-125 fragment (Ahn et al., 2020) (Figure 3.8C). The lamin aggregates were deposited near the perinuclear regions in the cells expressing the L59R mutant lamin A/C (Ahn et al., 2019a). Thus, the experiment was performed with the ACN mode assay using the L59R-harboring lamin 1-300 fragments to investigate the L59R mutation in phosphorylation at the N-terminal head region of the lamin. The phosphorylation at the N-terminal head region of the lamin fragment did not abolish the ACN interaction, unlike the wild-type lamin fragment. These findings suggest that the genetic mutation L59R overwhelms the CDK1 function of the phosphorylation-dependent perturbation of the ACN interactions in the lamin filaments, which may explain the perinuclear deposition of the lamin filaments by the mutation (Figure 3.9).

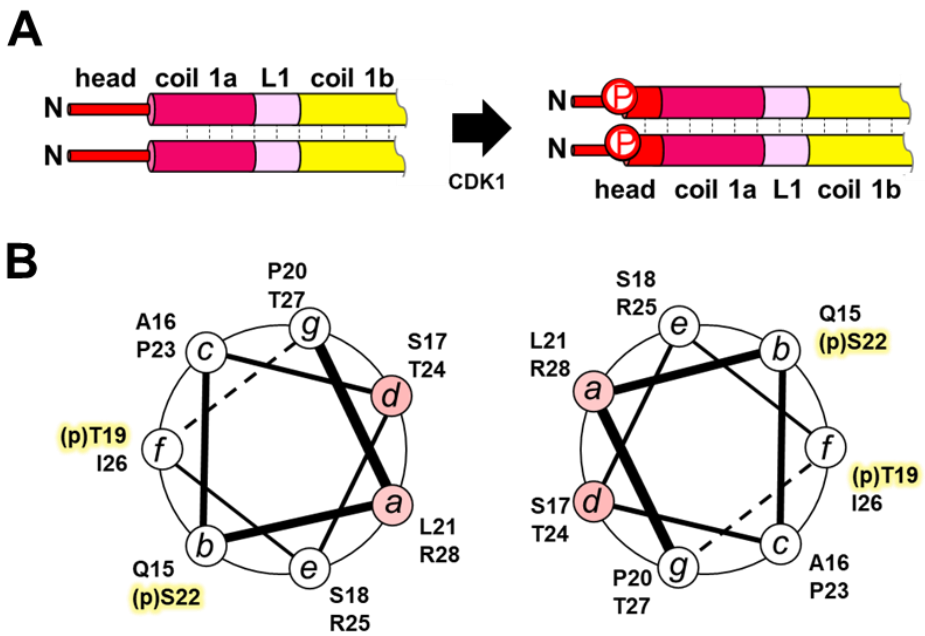

Figure 3. 6. A hypothesis when the Thr19 and S22 phosphorylated

A. A hypothesis representing the phosphorylation-dependent change in the coiled-coil propensity of the coil 1a region is presented with a schematic drawing of the lamin 1-125 fragment. P in the circles indicates the phosphorylated Ser/Thr. The thick cylinders represent the α-helices and the thin cylinders represent the unstructured region. The coiled-coil interactions are represented as dotted lines between the α-helical regions. Note that the phosphorylation expands the coil 1a α-helical regions to the N-terminal head region. **B.** The diagram using the heptad positions of the primary sequence and helical wheel plot. The residues are marked next to the corresponding heptad repeat position and the position described in italic (a to g). The position of a and d represented the red circle, and phosphorylation residues were colored yellow.

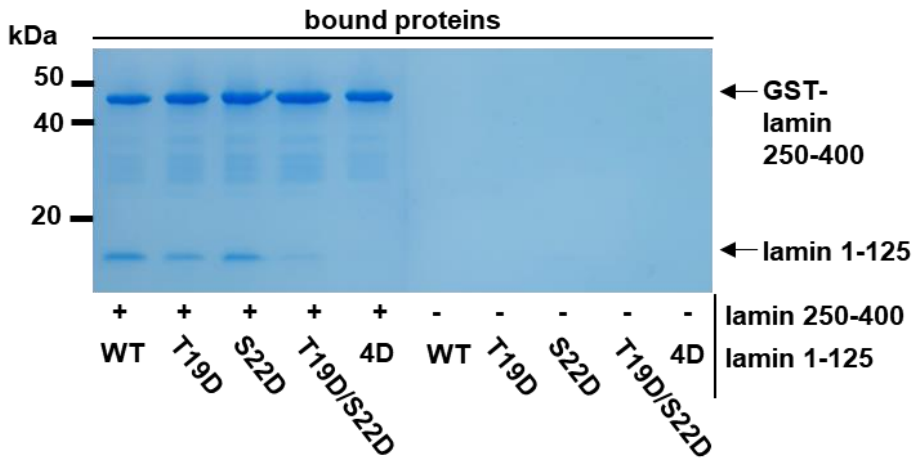

Figure 3. 7. Performing GST pull-down assays using mutations that mimicking thel lamin phosphorylation

GST pull-down assay between GST-fused lamin 250 to 400 and the mutant proteins of the lamin 1 to 125 fragment and further analysed by SDS-PAGE. The lamin 1 to 125 fragment mutations are labeled under the lane. “4D” stands for the quadruple mutation T10D/S12D/T19D/S22D. CDK1, cyclin-dependent kinase 1; GST, glutathione-S-transferase.

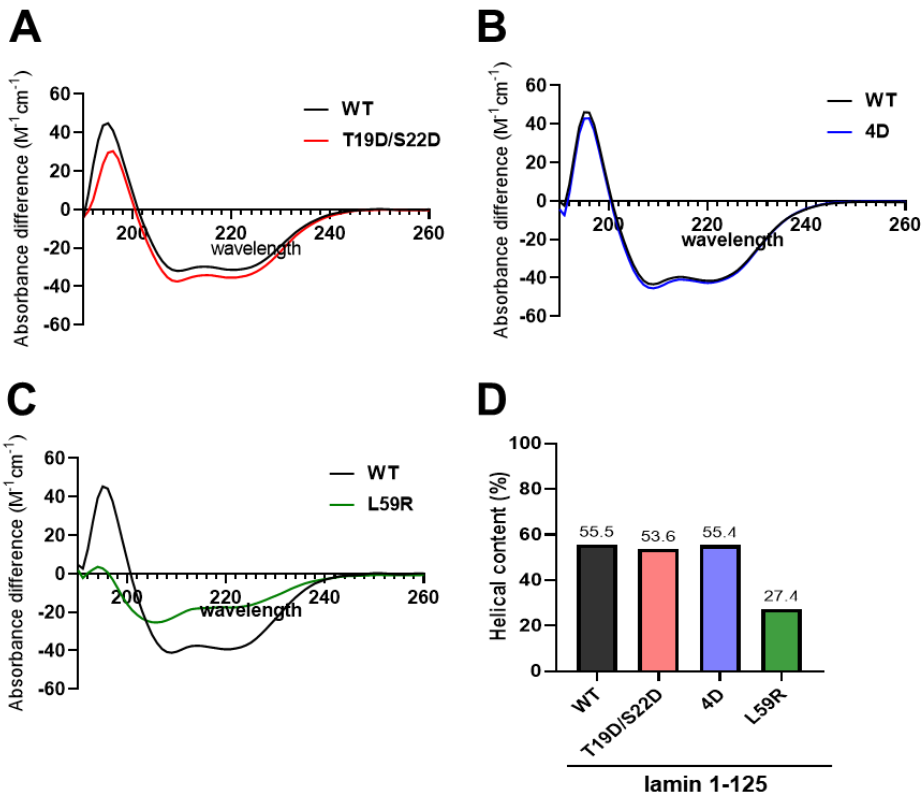

Figure 3. 8. The CD spectra of the wild-type and mutant lamin 125 fragments

A. The CD spectra (left) of the wild-type (black) and T19D/S22D mutant (red) lamin 125 fragments (1 mg/ml) **B.** The CD spectra (left) of the wild-type and 4D mutant (blue) lamin 125 fragments (1 mg/ml) **C.** The CD spectra (left) of the wild-type and L59R mutant (green) lamin 125 fragments (1 mg/ml) **D.** the helical contents from the CD spectra of the WT and mutant lamin 1 to 125 fragments. The portions of the secondary structure elements were analyzed by the CDNN software (Bohm et al., 1992).

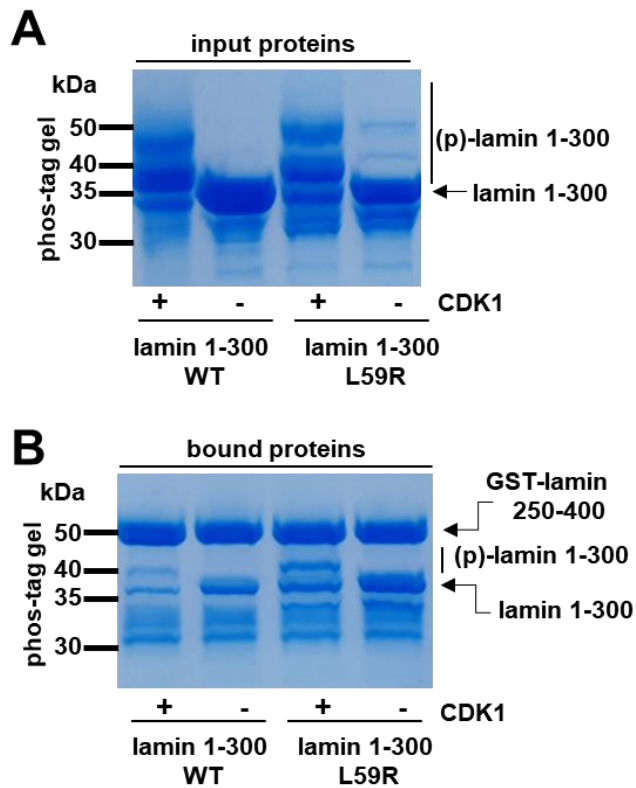

Figure 3. 9. GST pull-down assay between GST-fused lamin coil 250 to 400 and WT or L59R mutant lamin

A. GST pull-down assay between GST-fused lamin coil 250 to 400 and WT or L59R mutant lamin 1 to 300 fragments on a Phos-tag–containing SDS-polyacrylamide gel. The (un)phosphorylated WT and L59R lamin 1 to 300 fragments were prepared for the GST pull-down assay (input proteins). The phosphorylated lamin 1 to 300 ((p)-lamin 1 to 300) was upshifted on the gel (CDK1 + lanes). **B.** The (un)phosphorylated proteins were loaded on the GST-lamin coil 250 to 400–bound resin and then analyzed by the Phos-tag–containing SDS-polyacrylamide gel (bound proteins). CDK1, cyclin-dependent kinase 1; GST, glutathione-S-transferase.

3.3.4. Synergistic effects of the other cellular kinases with CDK1 activity on lamin

Cellular casein kinase 1 (CK1) and glycogen synthase kinase-3-β (GSK3β) are activated in cells and act on preferential sites of the prephosphorylated Ser/Thr sites (pS/pT) (Adhikari et al., 2012; Machowska et al., 2015). CK1 can preferentially act on Ser or Thr of the sequence (pS/pT)XX(S/T), where the underlined Ser or Thr is the target site, and GSK3β can act on the sequence (S/T)XXX(pS/pT) (Beurel et al., 2015; Flotow et al., 1990; Meggio et al., 1991). Due to the characteristic activities of CK1 and GSK3β, these two kinases increase the phosphorylation in adjacent regions of the prephosphorylation sites by the other kinase. To examine the cooperative action of CK1 and GSK3β with the CDK1/cyclin B complex, the recombinant CK1 and/or GSK3β proteins were incubated with the lamin N-terminal fragments (Figure 3.10). Without the CDK1 complex, CK1 and GSK3β treatment alone failed to abolish the ACN interaction. However, the cotreatment of CK1 and/or GSK3β with the CDK1 complex had synergistic effects on the attenuation of the ACN mode. These results suggest that the negative charges developed by phosphorylation are significant in attenuating the ACN and further present a possibility in which the other cellular kinases amplify the phosphorylation signal by CDK1.

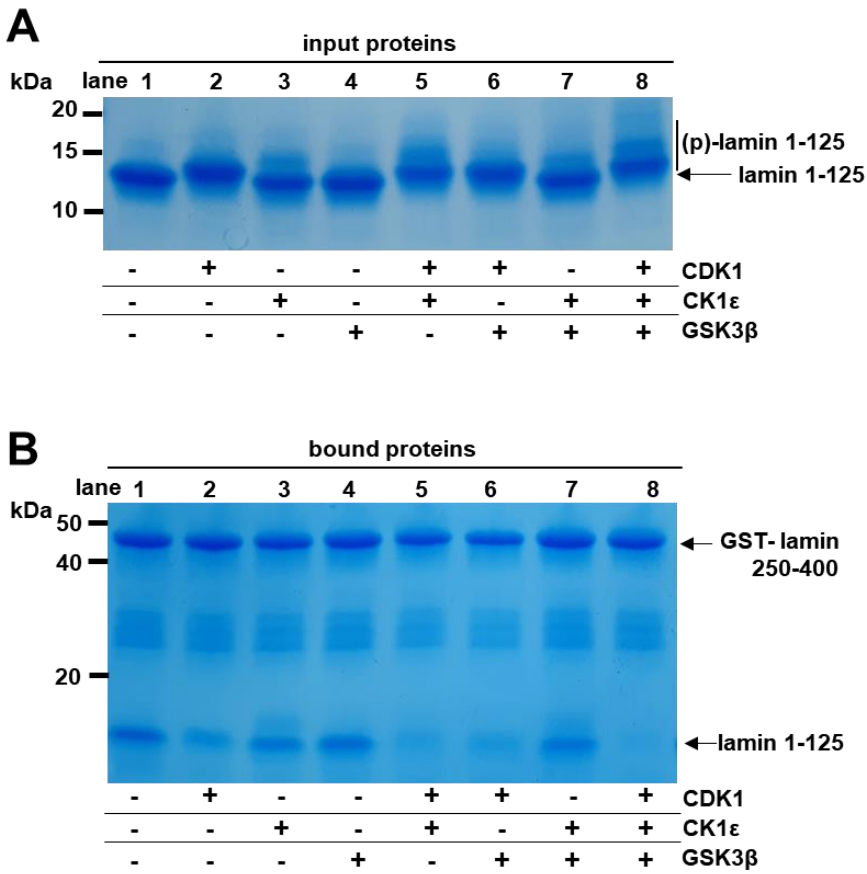

Figure 3. 10. The roles of phosphorylation by CK1 and GSK3β

A. The SDS-polyacrylamide gel was used to analyze the phosphorylation of input proteins of lamin 1 to 125 fragments by CDK1, CK1ε, and/or GSK3β. **B.** A GST pull-down assay was carried out to measure the ACN interaction using the GST-fused lamin coil 250 to 400. The lamin 1 to 125 fragment was phosphorylated by CDK1, CK1ε, and/or GSK3β and then loaded onto the GST-lamin 250 to 400–bound resin. The same amounts were used for CK1 ε, GSK3 β, and CDK1. Each sample was analyzed by SDS-PAGE.

3.3.5. The importance of the ionic interaction in the ACN binding

The experiment was performed to determine whether the ionic interaction is important in the interaction between coil 1a and coil 2 regions to gain molecular insight into the phosphorylation-dependent dissociation of the ACN mode. Since most ionic interactions are broken at high pH due to the absence of electrostatic charges at Lys and Arg, the binding of coil 1a and coil 2 was measured using the lamin 1-125 fragment and lamin 250-400 fragment at pH 9.5. The GST-lamin coil 250-400 fragment was linked covalently to the cyanogen bromide (CNBr)-activated resin to prevent the dissociation of the GST-fusion protein and GSH-resin at a high pH. The results showed that the high pH condition abolished the binding of coil 1a and coil 2 (Figure 3.11), indicating that ionic interactions are involved in ACN bonding. Arg25 and Arg28 were noted as two basic residues in the coil 1a region adjacent to the phosphorylation sites Thr19 and Ser22 in the chimeric structure of coil 1a (Stalmans et al., 2020). The R25E/R28E double mutation abolished the binding of coil 1a and coil 2, as shown in Figure 3.12, suggesting the importance of the basic residues for the ACN.

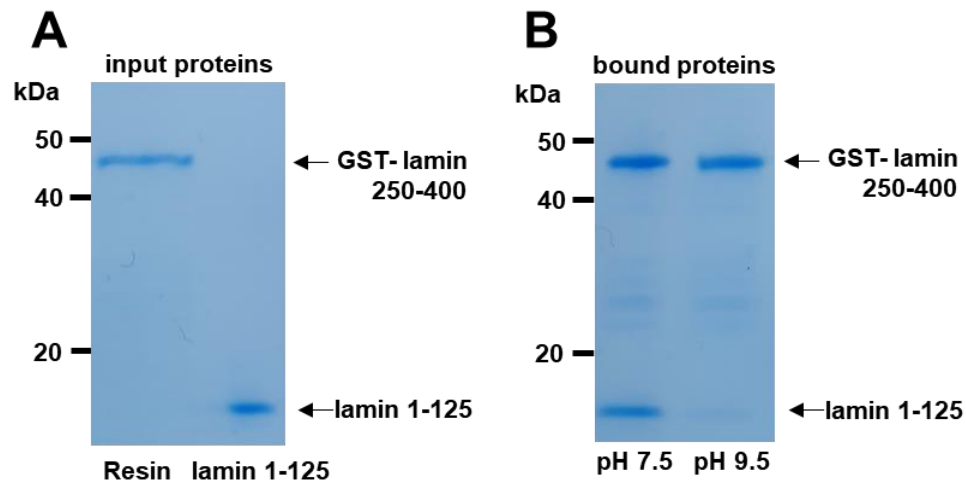

Figure 3. 11. Comparison the ACN interaction in pH 7.5 and pH 9.5 buffer

A. The input proteins were shown by SDS-PAGE **B.** Comparison of the ACN interactions between pH 7.5 and pH 9.5. GST-fused lamin 250 to 400 (GST-lamin coil 250–400) were covalently attached to the CNBr-activated resin, and then the lamin 1 to 125 fragment was incubated at the given pH. CNBr, cyanogens bromide; GST, glutathione-S-transferase.

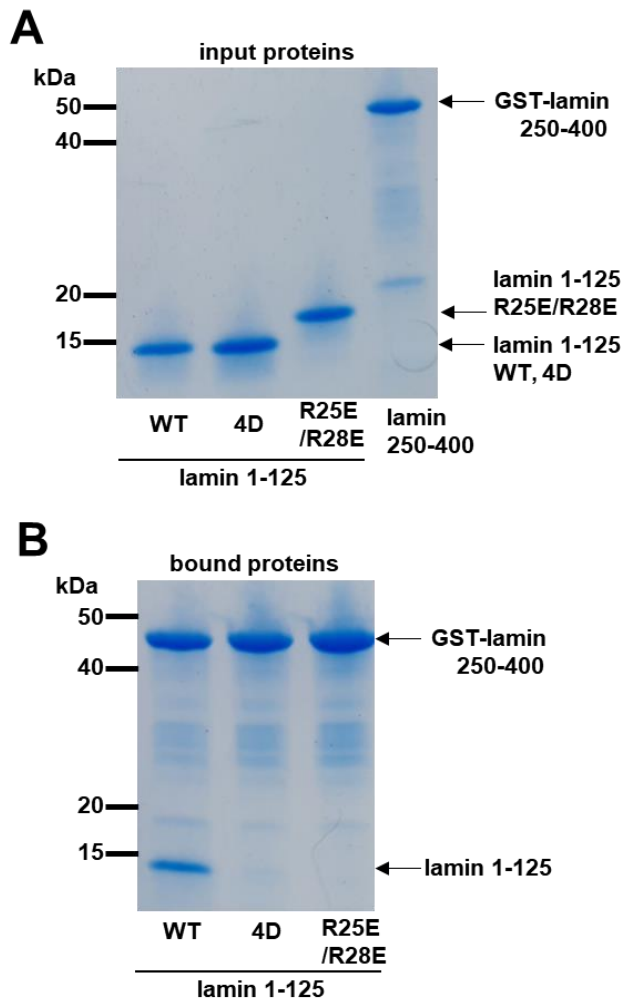

Figure 3. 12. Biochemical analysis of the ACN interaction using the GST-lamin coil 250 to 400 and the lamin 1 to 125 fragment

A. GST pull-down assay to test the importance of Arg25 and Arg28 in ACN interaction. All the proteins for the assay were prepared at the same concentration. **B.** The lamin 1 to 125 fragments (WT, 4D, or R25E/R28E) were incubated with GST-lamin 250 to 400–bound GSH-coupled resins, and then the bound proteins were analyzed by SDS-PAGE (bound proteins, the right panel).

3.4. Discussion

Cell cycle-dependent morphological changes in the nucleus are essential for understanding life phenomena at the molecular level. The phosphorylation levels of lamins are elevated 4- to 7-fold during mitosis than at interphase (Simon and Wilson, 2013). In this study, the pull-down assays demonstrated that phosphorylation at the lamin N-terminal head region abolishes the interaction of the C-terminal part of coil 2 and coil 1a, previously designated as the ACN (Makarov et al., 2019). The CDK1/cyclin B target sites Thr19 and Ser22 are critical in regulating the ACN mode. The multiple phosphorylation events in the head region additively contributed to the dissociation of the ACN without changing the coiled-coil propensity of the coil 1a region. In a previous study, the phosphorylation of S390 and S392 in the proximal C-terminal region before the Ig-like domain motif is also associated with the lamin filament disassembly (Kochin et al., 2014). The possibility of the involvement of other kinases was also presented, such as CK1 and GSK3β for multiple phosphorylation events. The molecular reason for properly forming the nuclear membrane in the laminopathy mutants was further provided.

Then, it was tried to determine how phosphorylation in the N-terminal head domain promotes the dissociation of the binding between coil 1a and the C-terminal part of coil 2. The complex model of coil 1a and a C-terminal part of coil 2 was built by Stalmans et al. (Stalmans et al., 2020), based on the individual proteins' structures (Figure 3.13). Stalmans et al. (Stalmans et al., 2020) made a parallel four-helix bundle model, which matched the cross-linking mass analysis by

Makarov et al. (Makarov et al., 2019). The previous results further supported the four-helix bundle formation that the separation of coil 1a and the C-terminal part of coil 2 was required (Ahn et al., 2020). The coiled-coils were separated for the structural transition from two coiled-coil dimers to the complex. To better estimate the role of phosphorylation in the N-terminal head region, this study created a similar complex model of the ACN mode, including the N-terminal head region. This model showed that the N-terminal head region folds back to coil 1a, supported by the cross-linking mass analysis (Makarov et al., 2019). According to the model refined by GalaxyRefineComplex (Heo et al., 2016), Arg25 and Arg28 form an ionic interaction network with the conserved Glu330 residue of the stutter region in the central cavity of the four-helix bundle (Figure 3.13A). This structural arrangement stabilizes the four-helix bundle structure at its end.

Based on these findings, a phosphorylation-dependent dissociation mechanism is proposed for the lamin filaments. The lamin filaments are stabilized by the intramolecular ACN mode between coil 1a and coil 2 via the Glu330 and Arg25/Arg28 residues during the interphase (Figure 3.13B, left). In the mitosis phase, the activated CDK1/cyclin B complex phosphorylates the N-terminal head region, forming an intramolecular ionic interaction with the basic residues of the coil 1a parts. These intramolecular ionic interactions disrupt the intermolecular ionic interaction network with the Glu residues at the end of the four-helix bundle structure (Figure 3.13B, right). Thus, coil 1a in the model used in this study serves as a pivot in the ACN mode between forming the intermolecular ionic interaction with coil 2 and the intramolecular interaction with the phosphorylated head region.

This disassembly of the ACN mode would finally trigger the depolymerization of the lamin filaments.

The phosphorylation state of the N-terminal head region of lamin regulates the cell cycle-dependent morphological change in the nuclear envelope. Therefore, the biochemical roles of phosphorylation in the context of the lamin complex structure are needed to understand its precise mechanism. This study has revealed the biochemical roles of phosphorylation in the depolymerization of lamin filaments. Furthermore, these results will help elucidate the cell cycle-dependent regulation of the nuclear shape, a fundamental phenomenon in all eukaryotic cells.

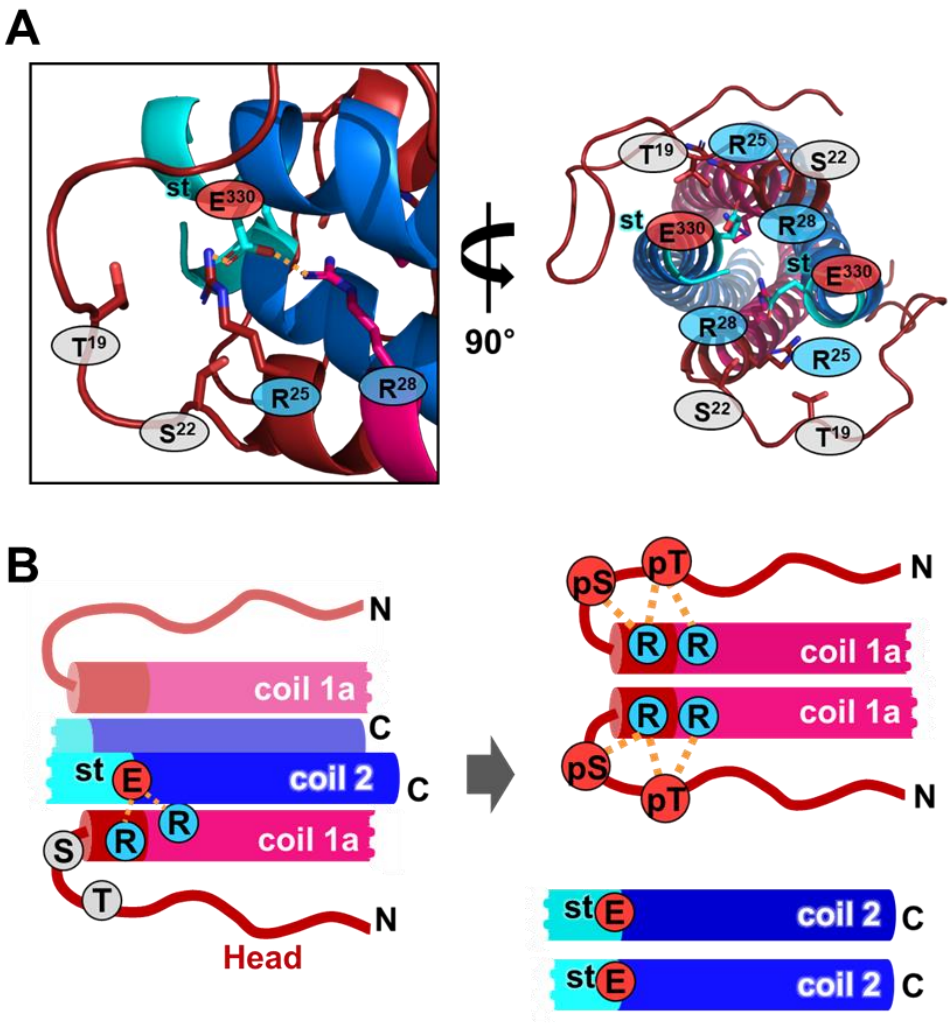
A
st
E330
T19
R25
R28
S22
90°
T19
R25
S22
st
E330
R28
st
E330
R28
R25
S22
T19
B
N
coil 1a
C
st
E
coil 2
C
S
R
R
coil 1a
T
N
Head
pS
pT
N
R
R
coil 1a
R
R
coil 1a
pS
pT
N
st
E
coil 2
C
st
E
coil 2
C

Figure 3. 13. A proposed mechanism of lamin depolymerization by phosphorylation

A. A model represents the ACN mode between coil 1a (magenta) and coil 2C (blue). The N-terminal head region (residues 1–27) was built by AlphaFold 2 (Jumper et al., 2021). The four-helix bundle region (residues 28–80 and 327–385) was built from the Stalmans et al. (Stalmans et al., 2020) model based on the typical four-helix bundle structure. The combined structure was refined by GalaxyRefineComplex (Heo et al., 2016). The ionic interaction network (yellow dotted lines), consisting of Arg25, Arg28, and stGlu330 (Glu330 at Stutter) (stick representations), was found near Thr19 and Ser22 (stick representations). The circle is colored to indicate the charge of residue (red, negatively charged residue; blue, positively charged residue; and gray, Thr19 and Ser22 residues). **B.** A proposed mechanism of lamin depolymerization. During interphase, the ACN is stabilized by the ionic interaction network (left). CDK1 activity during mitosis builds up the negative charges at the phosphorylation sites Thr19 and Ser22 (right). Then, the negative charges may compete and disrupt the ionic interaction network between coil 1a and the C-terminal region of coil 2, leading to the disassembly of the lamin filaments. CDK1, cyclin-dependent kinase 1.

Chapter 4.

The flavonoid alleviates incorrect lamin assemblies by interrupting the ACN interaction of lamin A

4.1. Introduction

Among the nuclear envelope consisting of proteins that organize the nucleus, nuclear lamin has two types: A and B; each forms a network structure under the inner membrane of the nucleus and maintains a frame of the cell nucleus (Gonzalez-Cruz et al., 2018). Recent studies have revealed that lamin interacts with the cytoskeleton in the cytoplasm through LINC proteins and the nuclear membrane to maintain the overall cellular form and exhibits resistance against mechanical stress (Vahabikashi et al., 2022). Kinases phosphorylate this compact nuclear layer mesh structure during cell division, and the nuclear layer is dissociated. When lamin forms a filament, it is elongated through a head-tail domain interaction called ACN interaction. The ACN interaction between the various interactions forming the filament structure during the decomposition process of the laminate is affected by phosphorylation (Jeong et al., 2022). Therefore, if there is a problem with ACN binding, normal separation does not occur during cell division, and the nucleus shape deforms.

Laminopathies are human diseases caused by genetic mutations in lamin (Coombs et al., 2021). Studies have revealed that mutations in coil 1a among laminopathies induce abnormal ACN interaction by biochemical study (Ahn et al., 2020). Moreover, lamin L59R mutation causes cardiomyopathy and Malouf syndrome in muscular dystrophy, and its cellular phenotype appears to be a deformation of the cell nucleus.

Flavonoids are natural products with a phenol structure and are known to play a role in antioxidants and anti-mutagenic properties (Panche et al., 2016).

These anti-mutagenic characteristics of flavonoids have also shown efficacy in HGPS, an aging disease caused by problems with the zmpste24 cleavage site in the pre-lamin processing where the resulting progerin is bound with the Ig-like domain of lamin. (Ahn et al., 2021c). In addition, muscle cells are sensitive to the oxidized isotropic imbalance caused by reactive oxygen species (ROS) produced by muscle contraction, and antioxidant therapy helps treat laminopathies that cause ROS (Coombs et al., 2021). This study found that flavonoids could ameliorate both laminopathies and aging.

4.2. Materials and Methods

4.2.1. Protein expression and purification

A previous study used the recombinant GST-fused coil 2 domain of lamin A (residues 250−400) and N-terminal hexahistidine tagged lamin A coil 1 L59R (residues 1−125) (Jeong et al., 2022). The transformed cells were cultured in 1 L Terrific broth at 37°C overnight, then 0.5 mM IPTG was added to overexpress the proteins. The cells were harvested by centrifugation and resuspended in a lysis buffer containing 20 mM Tris-HCl pH 8.0 and 150 mM NaCl. The resuspended cells were disrupted using a French press, and the cell debris was removed by centrifugation. The supernatants were loaded onto the proper resin (GSH-conjugated resin for GST-fused protein and nickel resin for his-tagged protein). After performing affinity chromatography using the standard procedure, the eluent was further purified by anion exchange chromatography (HiTrap Q HP, Cytiva, USA). The purified proteins were stored at -80°C.

4.2.2. ELISA

ELISA (The Enzyme-linked immunosorbent assay) was performed using a GSH-coated 96-well plate to explore natural inhibitors that interfere with abnormal ACN binding of lamin L59R mutant proteins. GST-fused lamin A 250-400 was fixed on a GSH-coated 96-well plate (Thermofisher, USA) at room temperature (RT) for an hour, and then the residue was removed using a PBS buffer containing 0.1% BSA, 0.5 mM EDTA, and 0.02% tween 20. His-tagged lamin A1-125 L59R and 5 mM natural compounds were incubated at RT for an hour, and then anti-

GST-Ab (1:500, Santacruz, USA) and anti-mouse IgG-HRP (1:5,000, Santacruz, USA) were treated sequentially for two hours. After washing the 96-well plate, the interaction between the two proteins is detected by TMB solution (Calbiochem, USA) and added stop solution (0.1 N H2SO4). The absorbance of these reactions was determined at 450 nm.

4.2.3. Molecular docking and molecular dynamics simulation studies

The molecular docking of lamin ACN interaction complex with some flavonoids (morin, baicalein, fisetin, and apigenin) was calculated by the Autodock-GPU program (Dallakyan and Olson, 2015). The macromolecular structure of the lamin ACN complex was designed by alphafold2, which was used in a previous study. The flavonoid structures as ligands were downloaded at PubChems in the SDF format (Pubchem IDs: 5281670, 5281605, 5281614, and 5280443). To further refine the docked structure, GROMACS software was used for molecular dynamics (MD) simulation (Pronk et al., 2013). The force field for the aqueous solvent environment was obtained using CHARMM-GUI, and the water box size was set based on the longest side of the structure, 120 Å and adding 150 mM NaCl molecules (Cheng et al., 2013; Qi et al., 2014). The MD simulation was performed for 100 ns using GROMACS, and the results were visualized by the PyMOL program (Schrodinger, 2015).

4.2.4. Human fibrosarcoma cell culture and flavonoid treatment

HT1080 cell line were cultured in liquid medium (DMEM) containing 10% (v/v) FBS, 1% (v/v) antibiotics at 37°C. HT1080 cells were seeded on a cover glass

and transfected with the plasmid coding L59R mutant of full-length lamin A/C fused with GFP using LipofectamineTM 3000 (Enzynomics, USA). After transfection, cells were incubated for 24 hours in liquid medium containing 2% (v/v) FBS, 1% antibiotics, and 100 μM flavonoid at 37°C. The immunofluorescence signal in the cells was detected using fluorescence microscopy.

Table 4. 1. Complete list of the natural compound library

No.	Name	Supplier	Country
1	Erythritol	LiftMode	IL, USA
2	Curcumin	LiftMode	IL, USA
3	Dihydromyricetin	LiftMode	IL, USA
4	Matrine	LiftMode	IL, USA
5	Phenylpiracetam	LiftMode	IL, USA
6	Synephrine	LiftMode	IL, USA
7	D-quinic acid	NOW Foods	IL, USA
8	Inositol	LiftMode	IL, USA
9	Pyridoxine-HCL	LiftMode	IL, USA
10	Magnolol	LiftMode	IL, USA
11	Alpha-lipoic acid	LiftMode	IL, USA
12	Acetyl L-Carnitine HCL	Sigma	MA, USA
13	L-Tryptophan	LiftMode	IL, USA
14	Piperine	LiftMode	IL, USA
15	5-HTP	LiftMode	IL, USA
16	Ursolic acid	Sigma	MA, USA
17	Baicalein	LiftMode	IL, USA
18	L-Tetrahydropalmatine	LiftMode	IL, USA
19	Yohimbine HCL	LiftMode	IL, USA
20	Vanillin	Sigma	MA, USA
21	Morin	Sigma	MA, USA
22	Betaine HCL	NOW Foods	IL, USA
23	Vitamin C	NOW Foods	IL, USA

24	Xylitol	LiftMode	IL, USA
25	Niacin	LiftMode	IL, USA
26	Apigenin	LiftMode	IL, USA
27	Inosine	Sigma	MA, USA
28	Baicalin	LiftMode	IL, USA
29	EGCg	NOW Foods	IL, USA
30	Rutin	LiftMode	IL, USA
31	D-Raffinose pentahydrate	Dae Jung	Korea
32	Menthol	Sigma	MA, USA
33	p-Coumaric acid	Sigma	MA, USA
34	Cinnamic acid	Sigma	MA, USA
35	Resveratrol	LiftMode	IL, USA
36	Noopept	NOW Foods	IL, USA
37	Lactic acid	Dae Jung	Korea
38	Gallic acid monohydrate	Dae Jung	Korea
39	N-acetyl-cystein	LiftMode	IL, USA
40	Choline bitartrate	LiftMode	IL, USA
41	Hordenine HCL	LiftMode	IL, USA
42	L-carnitine fumarate	Doctor’s Best	CA, USA
43	Phenylethylamine HCL	LiftMode	IL, USA
44	Quercetin	Jarrow Formulas	CA, USA
45	Fisetin	LiftMode	IL, USA
46	Kaempferol	Violet Herbs	USA

4.3. Results

4.3.1. Screening of inhibitory compound for abnormal ACN interactions in nuclear lamin L59R mutant

The mutation converted leucine 59th residue to arginine in lamin A, which is one of the gene mutations related to muscular dystrophy that exhibits abnormal ACN interactions from longitudinal head-to-tail interaction, as previous studies have revealed. These unusual interactions fail to completely disassemble the meshwork of nuclear lamin during mitosis, resulting in blebbing phenotypes in cells. Therefore, screening was conducted to find a compound that could weaken this excessive interaction. The compounds used in this experiment were edible natural products, described in detail in Table 4.1.

The his-tagged lamin 1-125 L59R and GST-fused lamin A 250-400 used to exhibit the ACN binding of lamin A was attached to the GSH-coated plate, and then the ELISA experiment was designed using a his-tag antibody. It showed that the binding ratio of ACN interaction was only lower in four out of the 43 natural compounds: baicalein, L-tetrahydropalmatine, morin, and menthol (Figure 4.1). Most of the substances derived through screening belong to flavonoids, and the previous study has shown that Morin is effective in HGPS, where abnormal lamin binding is induced by progerin (Ahn et al., 2021c). Thus, eight flavonoids were selected that easily gained as an edible supplement in the market, and there were tested at two concentrations (200 μM and 100 μM) to exhibit whether flavonoids are helpful even in the interference of abnormal binding of L59R-induced laminopathy.

Most substances contributed to preventing the strong binding of the L59R mutant except quercetin. Among the other seven flavonoids, morin was most effective in interfering with the ACN interaction derived in the L59R mutant. All the flavonoids used in screening are classified as flavone and flavonol, except L-tetrahydropalmatine, but their effectiveness varies depending on the hydroxyl location. According to the result of flavonoid screening, morin was most effective at 0.1 mM concentration (Figure 4.2). Also, baicalein, fisetin, and apigenin had the potential to interfere with the abnormal interaction of head-to-tail interaction of lamin. This screening showed the possibility of specific pharmacological properties from flavonoids.

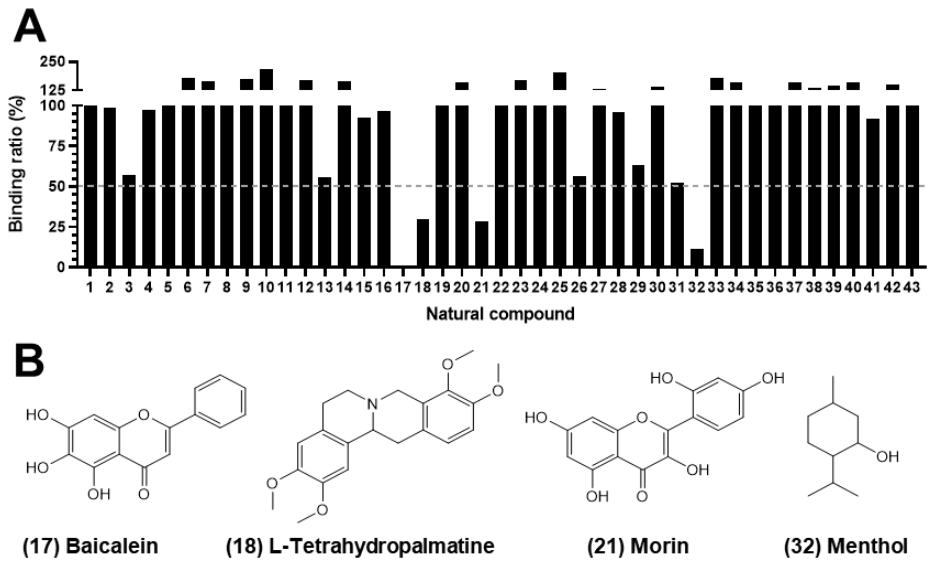

Figure 4. 1. Screening the abnormal ACN interaction due to L59R mutation in coil 1 of lamin A using natural compounds

A. Performing the ELISA screening using the natural compound described in Table 4.1. The left axis represents the binding ratio of ACN interaction between his-tagged lamin A 1-125 L59R and GST-tagged lamin A 250-400. **B.** The natural compounds were selected by ELISA. (17) Baicalein, (18) L-tetrahydropalmatine, (21) Morin, and (32) Menthol.

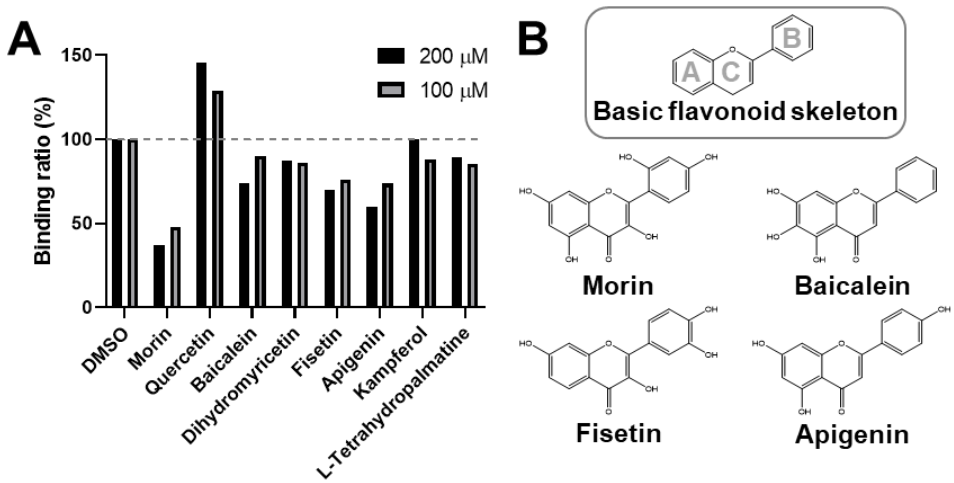

Figure 4. 2. ELISA screening using the flavonoids

A. Performing the ELISA screening using the flavonoids. The left axis represents the binding ratio of ACN interaction between his-tagged lamin A 1-125 L59R and GST-tagged lamin A 250-400. **B.** The structure of the basic flavonoid skeleton is represented in a grey box. The structure of flavonoids which ELISA selected. The morin and fisetin are containing the flavonol and baicalein and apigenin are in flavone.

4.3.2. Predicting the effect of flavonoids on abnormal interaction of lamin A

Molecular docking and MD simulation were further attempted to predict whether flavonoids could interact directly with lamin A (Figure 4.3). The complex structure of lamin A, which showed ACN interaction, was obtained from Alphafold2. Then, autodock-GPU in PyRx virtual screening software was used to find four flavonoids that were deemed effective through experimentation with ELISA: morin, baicalein, fisetin, and apigenin. As a result of the docked structure, all flavonoids are located between coil 1a and the head of lamin A. This region is where the residues, mainly phosphorylated, are gathered in the dispersion of lamin A, and also the surface of this region showed hydrophilic (Figure 4.3A).

The flavonoid structure comprises two phenylic rings and one heterocyclic ring (Figure 4.2 B). According to the molecular docking results, the B-ring of morin, fisetin, and apigenin is in a hydrophilic pocket made by the head domain of the lamin, but baicalein shows that the A-ring is located. These results seemed to rely on the presence or absence of a hydroxyl group of phenolic rings. According to the hydroxyl groups of the binding phenolic ring, that was reflected in the binding energy, morin had - 6.83 kcal·mol^{-1}, baicalein had - 6.28 kcal·mol^{-1}, fisetin had - 6.96 kcal·mol^{-1}, and apigenin had − 5.8 kcal·mol^{-1}.

After docking, a molecular dynamics (MD) simulation was performed using GROMACS software to predict the binding stability between flavonoids and lamin A structure (Figure 4.4). The MD simulation results' stability was shown by calculating the RMSD for each state. The scale over 1 Å from calculating the

RMSD indicated the escape of the water box of the ACN complex protein model. According to the MD simulation, all four flavonoids escaped for the head domain before 100 ns. Morin and fisetin are predicted that be stable for about 20 ns, but baicalein and apigenin are removed from the head domain before 10 ns. The difference in stability time to prediction for the two groups is that they were to belong to the category of flavonoid. The morin and fisetin belong to flavonol, and baicalein and apigenin are in flavone. The difference between these groups is the hydroxyl group on B-ring. Thus, flavonol, which had the additional hydroxylation in the B-ring, made a more stable result in the prediction between flavonoid and ACN complex of lamin in MD simulation.

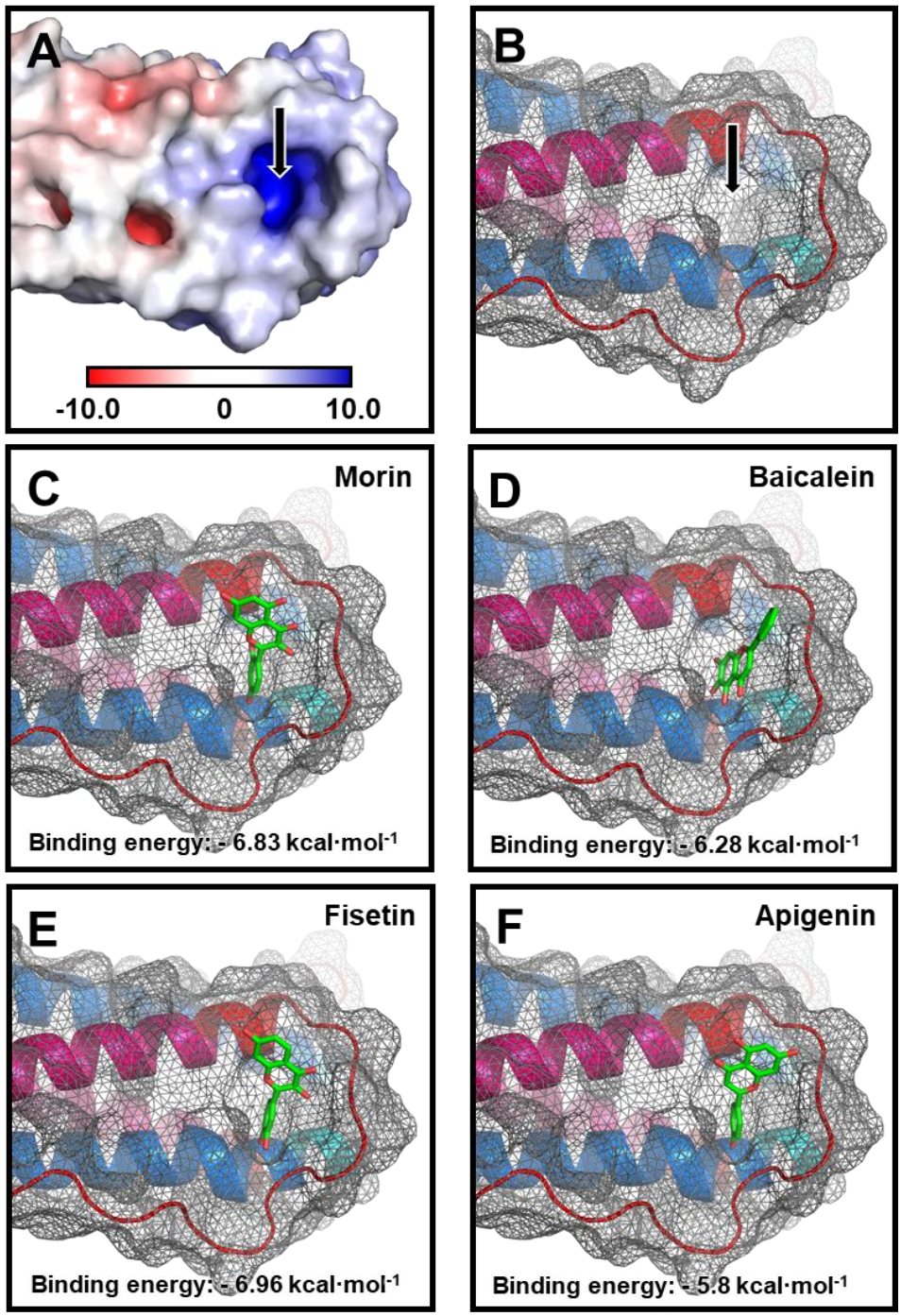
A
-10.0
0
10.0
B
C
Morin
Binding energy: - 6.83 kcal·mol-1
D
Baicalein
Binding energy: - 6.28 kcal·mol-1
E
Fisetin
Binding energy: - 6.96 kcal·mol-1
F
Apigenin
Binding energy: - 5.8 kcal·mol-1

Figure 4. 3. The results of molecular docking using the PyRx program

A. The electrostatic effect on the surface of the ACN complex model used for molecular docking. The electrostatic effect ranges from -10 to +10. The black arrow pointed to the pockets generated in the head domain in the complex model. B. The ACN complex model is represented by a cartoon, and each domain is colored, red shows the head, magenta shows coil 1a, blue shows coil 2, and cyan as a stutter in coil 2. A grey mesh represents the surface. As a result of molecular docking, each flavonoid was located in this pocket, pointed by an arrow. The flavonoids are represented by a green stick, and the binding energy for each flavonoid is represented below. **B.** Morin, **C.** Baicalein, **D.** Fisetin, **E.** Apigenin.

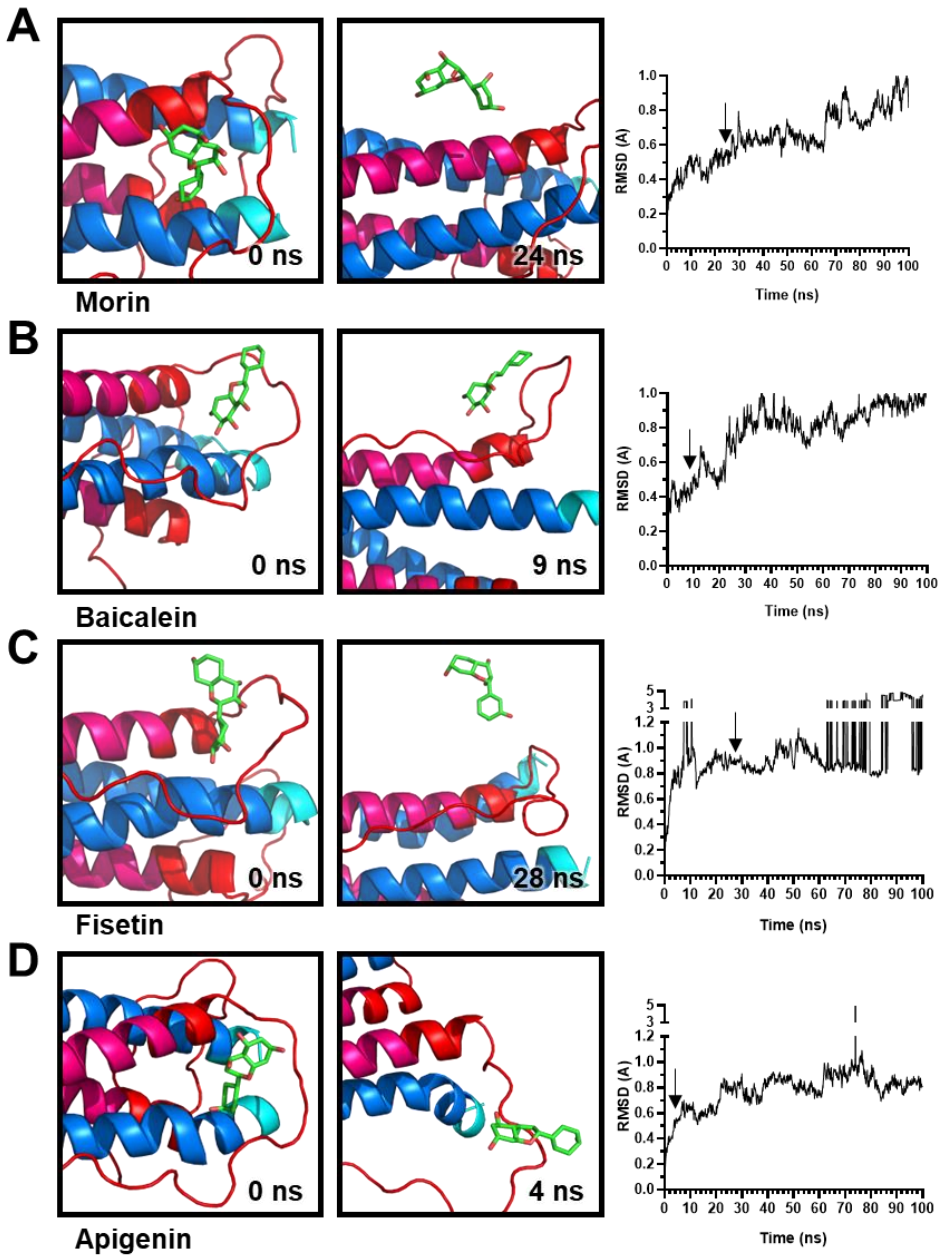
A
0 ns
24 ns
RMSD (A)
Time (ns)
Morin
B
0 ns
9 ns
RMSD (A)
Time (ns)
Baicalein
C
0 ns
28 ns
RMSD (A)
Time (ns)
Fisetin
D
0 ns
4 ns
RMSD (A)
Time (ns)
Apigenin

Figure 4. 4. The results of MD simulation by GROMACS

The MD simulation of lamin ACN complex with flavonoids. The macromolecular is presented by cartoons, and their colors show the domain of lamin A. The head domain, coil 1a, stutter, and coil 2 were colored respectively by red, pink, cyan, and blue. The flavonoids are represented as a stick and colored green. For each compound, the pre-MD simulation and post-MD simulation images were captured. When the MD simulation was performed was written in the lower right corner of the picture. The root means square deviation (RMSD) for protein stability during the simulation time is plotted in the right panel. The black arrow in the plot points to the point in time of the captured image. Flavonoids used in MD simulation are **A.** Morin, **B.** Baicalein, **C.** Fisetin, and **D.** Apigenin.

4.3.3. The flavonoid improves the nuclear deformation formed by an abnormal interaction

I examined whether the flavonoid treatment helps maintain regular nuclear shapes in HT1080 cells expressing the entire length of lamin A with L59R mutation. To show the nuclear envelope formation clearly, expressing lamin A fused GFP was transfected in HT1080. The phenotype of cells with L59R mutation in lamin A exhibited that the nuclear envelope was not smooth, and aggregation occurred partially on the nuclear surface (Figure 4.5). After expressing the mutant lamin, the shapes of the nucleus in cells treated with morin, baicalein, fisetin, and apigenin were compared. The overall shape of the nucleus of the morin-treated HT1080 cells was spherical, and the aggregation of the nuclear envelope was reduced. On the other hand, baicalein, fisetin, and apigenin showed similar phenotypes to cells treated with DMSO. Thus, this result showed the possibility that morin could ameliorate the abnormal ACN interaction of the lamin filaments resulting from a single gene mutation in lamin A.

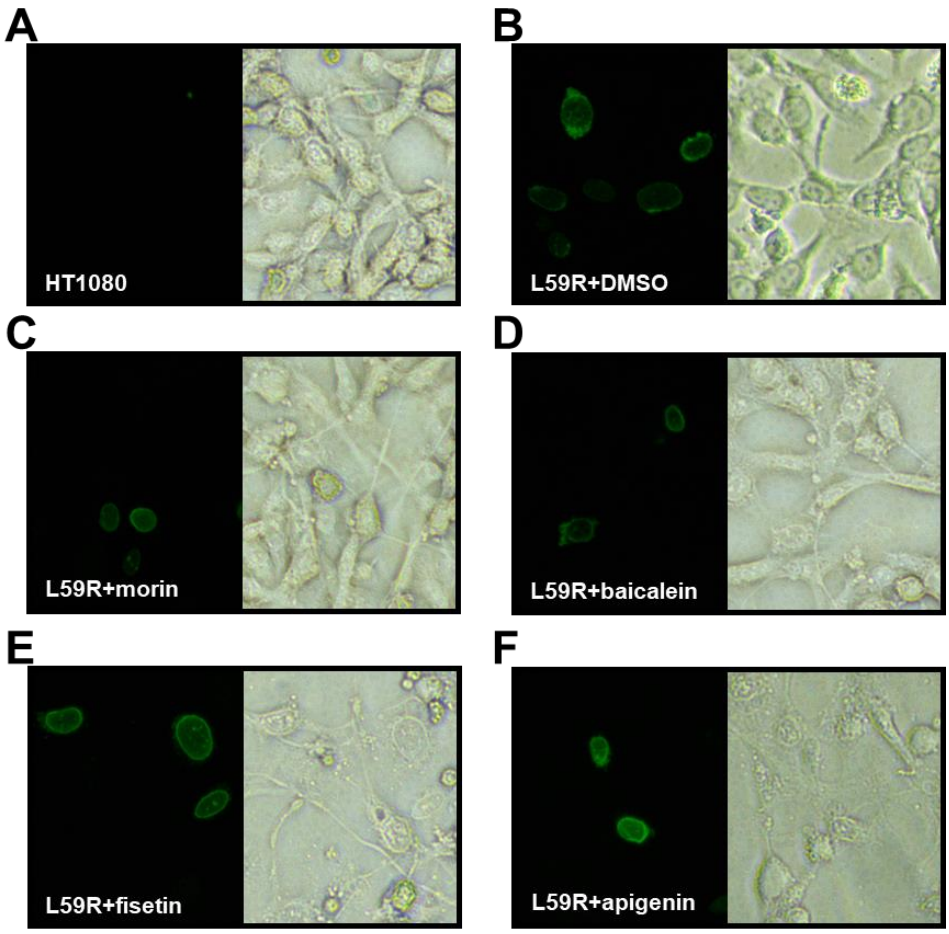
A
HT1080
B
L59R+DMSO
C
L59R+morin
D
L59R+baicalein
E
L59R+fisetin
F
L59R+apigenin

Figure 4. 5. The nuclear morphology of the L59R of lamin A/C after treating flavonoids

After treating 100 μM flavonoids for 24 hours, the shape and distribution of the nucleus were observed using a fluorescence microscope. For visualization of the nuclear membrane, the GFP-fused lamin A harboring L59R mutation was transfected (green). The right panel shows us using a phase difference microscope to illuminate the entire state of the cell. **A.** This showed HT1080 cells without any gene transfection. **B.** After expressing the lamin A harboring L59R mutation on HT1080, the cell was treated with morin, **C.** baicalein, **D.** fisetin, and **E.** apigenin with 100 μM for 24 hours.

4.4. Discussion

The incomplete disassembly of lamin typically fails to form a nuclear shape after cell division and can directly affect the maintenance of life phenomena such as DNA damage. In this research, ELISA identified the possibility that flavonoids among various natural products may interfere with the abnormal binding to the L59R mutation of lamin. In addition, molecular docking and MD simulations predicted the pharmacological potential of flavonoids in the complex model of lamin A, where the model represented longitudinal interaction to form a lamin filament. Moreover, treatment of morin in HT1080 cells with L59R mutation of lamin A identified improved nuclear formation, and it was similar to the results predicted using MD simulation.

Both fisetin and morin, expected to interfere with abnormal ACN binding of lamin A effectively, belong to the plant flavonol and can be used as oral dietary supplements and have no reported side effects (Yousefzadeh et al., 2018). In clinical studies, the dose of fisetin is 20 mg/kg/day as a dietary supplement, and no side effects occurred even if sufficient doses were taken orally, about 200-800 mg as a capsule per day (Wang et al., 2022).

Quercetin, which also belongs to the flavonol and isomeric form of morin, is the most effective antioxidant and has a higher electron donor ability than morin and fisetin (Xu et al., 2019). However, it has not shown a result in reducing abnormal binding in the lamin filaments. The ELISA result of quercetin suggests that morin and fisetin are directly involved in the interaction between proteins rather than the role of anti-aging as anti-oxidants.

In addition, fisetin has reduced the senescent-associated secretory phenotypes (SASPs) as an aging marker in senescent cells to prolong the health and lifespan of the mouse (Yousefzadeh et al., 2018). Furthermore, it has been recently announced that morin already has a direct effect on the binding of lamin filament. Morin inhibits abnormal binding in progerin-induced HGPS (Ahn et al., 2021c).

The L59R mutation causes muscular dystrophy among laminopathies and appears in cardiomyopathy and Malouf syndrome (McPherson et al., 2009). Although finding a specific clinical treatment for laminopathies is difficult, this study shows that flavonoids can cooperate with the structural dispersion of nuclear lamina in laminopathies and the role of antioxidants. I believe that this result helps provide insights into the treatment of laminopathies.

Bibliography

Adhikari, D., Zheng, W., Shen, Y., Gorre, N., Ning, Y., Halet, G., Kaldis, P., and Liu, K. (2012). Cdk1, but not Cdk2, is the sole Cdk that is essential and sufficient to drive resumption of meiosis in mouse oocytes. *Hum Mol Genet* **21**, 2476-2484. 10.1093/hmg/dds061.

Aebi, U., Cohn, J., Buhle, L., and Gerace, L. (1986). The nuclear lamina is a meshwork of intermediate-type filaments. *Nature* **323**, 560-564. 10.1038/323560a0.

Aebi, U., Haner, M., Troncoso, J., Eichner, R., and Engel, A. (1988). Unifying Principles in Intermediate Filament (If) Structure and Assembly. *Protoplasma* **145**, 73-81. Doi 10.1007/Bf01349341.

Afonine, P.V., Grosse-Kunstleve, R.W., Echols, N., Headd, J.J., Moriarty, N.W., Mustyakimov, M., Terwilliger, T.C., Urzhumtsev, A., Zwart, P.H., and Adams, P.D. (2012). Towards automated crystallographic structure refinement with phenix.refine. *Acta Crystallogr D Biol Crystallogr* **68**, 352-367. 10.1107/S0907444912001308.

Ahn, J., Jeong, S., Kang, S.M., Jo, I., Park, B.J., and Ha, N.C. (2020). Separation of Coiled-Coil Structures in Lamin A/C Is Required for the Elongation of the Filament. *Cells* **10**. 10.3390/cells10010055.

Ahn, J., Jo, I., Kang, S.M., Hong, S., Kim, S., Jeong, S., Kim, Y.H., Park, B.J., and Ha, N.C. (2019a). Structural basis for lamin assembly at the molecular level. *Nature Communications* **10**. ARTN 375710.1038/s41467-019-11684-x.

Ahn, J., Jo, I., Kang, S.M., Hong, S., Kim, S., Jeong, S., Kim, Y.H., Park, B.J., and Ha, N.C. (2019b). Structural basis for lamin assembly at the molecular level. *Nat Commun* **10**, 3757. 10.1038/s41467-019-11684-x.

Ahn, J., Lee, J., Jeong, S., Kang, S.M., Park, B.J., and Ha, N.C. (2021a). Beta-strand-mediated dimeric formation of the Ig-like domains of human lamin A/C and B1. *Biochem Biophys Res Commun* **550**, 191-196. 10.1016/j.bbrc.2021.02.102.

Ahn, J., Woo, T.G., Kang, S.M., Jo, I., Woo, J.S., Park, B.J., and Ha, N.C. (2021b). The flavonoid morin alleviates nuclear deformation in aged cells by disrupting progerin-lamin A/C binding. *J Funct Foods* **77**. ARTN 10433110.1016/j.jff.2020.104331.

Ahn, J., Woo, T.G., Kang, S.M., Jo, I., Woo, J.S., Park, B.J., and Ha, N.C. (2021c). The flavonoid morin alleviates nuclear deformation in aged cells by disrupting progerin-lamin A/C binding (vol 77, 104331, 2021). *J Funct Foods* **87**. ARTN 10484310.1016/j.jff.2021.104843.

Beck, L.A., Hosick, T.J., and Sinensky, M. (1990). Isoprenylation Is Required for the Processing of the Lamin-a Precursor. *J Cell Biol* **110**, 1489-1499. DOI 10.1083/jcb.110.5.1489.

Bera, M., Ainavarapu, S.R., and Sengupta, K. (2016). Significance of 1B and 2B domains in modulating elastic properties of lamin A. *Sci Rep* **6**, 27879. 10.1038/srep27879.

Bercht Pfleghaar, K., Taimen, P., Butin-Israeli, V., Shimi, T., Langer-Freitag, S., Markaki, Y., Goldman, A.E., Wehnert, M., and Goldman, R.D. (2015). Gene-rich chromosomal regions are preferentially localized in the lamin B deficient nuclear blebs of atypical progeria cells. *Nucleus* **6**, 66-76. 10.1080/19491034.2015.1004256.

Beurel, E., Grieco, S.F., and Jope, R.S. (2015). Glycogen synthase kinase-3 (GSK3): regulation, actions, and diseases. *Pharmacol Ther* **148**, 114-131. 10.1016/j.pharmthera.2014.11.016.

Bidault, G., Vatier, C., Capeau, J., Vigouroux, C., and Bereziat, V. (2011). LMNA-linked lipodystrophies: from altered fat distribution to cellular alterations. *Biochem Soc Trans* **39**, 1752-1757. 10.1042/BST20110675.

Bohm, G., Muhr, R., and Jaenicke, R. (1992). Quantitative analysis of protein far UV circular dichroism spectra by neural networks. *Protein Eng* **5**, 191-195. 10.1093/protein/5.3.191.

Broers, J.L., Ramaekers, F.C., Bonne, G., Yaou, R.B., and Hutchison, C.J. (2006). Nuclear lamins: laminopathies and their role in premature ageing. *Physiol Rev* **86**, 967-1008. 10.1152/physrev.00047.2005.

Bunick, C.G., and Milstone, L.M. (2017). The X-Ray Crystal Structure of the Keratin 1-Keratin 10 Helix 2B Heterodimer Reveals Molecular Surface Properties and Biochemical Insights into Human Skin Disease. *J Invest Dermatol* **137**, 142-150. 10.1016/j.jid.2016.08.018.

Butin-Israeli, V., Adam, S.A., Goldman, A.E., and Goldman, R.D. (2012). Nuclear lamin functions and disease. *Trends Genet* **28**, 464-471. 10.1016/j.tig.2012.06.001.

Chen, J.T., Ho, C.W., Chi, L.M., Chien, K.Y., Hsieh, Y.J., Lin, S.J., and Yu, J.S. (2013). Identification of the lamin A/C phosphoepitope recognized by the

antibody P-STM in mitotic HeLa S3 cells. *BMC Biochem* **14**, 18. 10.1186/1471-2091-14-18.

Cheng, X., Jo, S., Lee, H.S., Klauda, J.B., and Im, W. (2013). CHARMM-GUI Micelle Builder for Pure/Mixed Micelle and Protein/Micelle Complex Systems. *J Chem Inf Model* **53**, 2171-2180. 10.1021/ci4002684.

Chernyatina, A.A., Guzenko, D., and Strelkov, S.V. (2015). Intermediate filament structure: the bottom-up approach. *Curr Opin Cell Biol* **32**, 65-72. 10.1016/j.ceb.2014.12.007.

Coombs, G.S., Rios-Monterrosa, J.L., Lai, S.P., Dai, Q., Goll, A.C., Ketterer, M.R., Valdes, M.F., Uche, N., Benjamin, I.J., and Wallrath, L.L. (2021). Modulation of muscle redox and protein aggregation rescues lethality caused by mutant lamins. *Redox Biol* **48**. ARTN 10219610.1016/j.redox.2021.102196.

Dallakyan, S., and Olson, A.J. (2015). Small-molecule library screening by docking with PyRx. *Methods Mol Biol* **1263**, 243-250. 10.1007/978-1-4939-2269-7_19.

Dessev, G.N., Iovcheva-Dessev, C., and Goldman, R.D. (1990). Lamin dimers. Presence in the nuclear lamina of surf clam oocytes and release during nuclear envelope breakdown. *J Biol Chem* **265**, 12636-12641.

Dittmer, T.A., and Misteli, T. (2011). The lamin protein family. *Genome Biol* **12**, 222. 10.1186/gb-2011-12-5-222.

Eldirany, S.A., Ho, M., Hinbest, A.J., Lomakin, I.B., and Bunick, C.G. (2019). Human keratin 1/10-1B tetramer structures reveal a knob-pocket mechanism in intermediate filament assembly. *EMBO J* **38**. 10.15252/embj.2018100741.

Eldirany, S.A., Lomakin, I.B., Ho, M., and Bunick, C.G. (2021a). Recent insight into intermediate filament structure. *Curr Opin Cell Biol* **68**, 132-143. 10.1016/j.ceb.2020.10.001.

Eldirany, S.A., Lomakin, I.B., Ho, M., and Bunick, C.G. (2021b). Recent insight into intermediate filament structure. *Curr Opin Cell Biol* **68**, 132-143. 10.1016/j.ceb.2020.10.001.

Emsley, P., and Cowtan, K. (2004). Coot: model-building tools for molecular graphics. *Acta Crystallogr D Biol Crystallogr* **60**, 2126-2132. 10.1107/S0907444904019158.

Erber, A., Riemer, D., Hofemeister, H., Bovenschulte, M., Stick, R., Panopoulou, G., Lehrach, H., and Weber, K. (1999). Characterization of the

Hydra lamin and its gene: A molecular phylogeny of metazoan lamins. *J Mol Evol* **49**, 260-271. 10.1007/pl00006548.

Fan, X., Fan, Z., Yang, Z., Huang, T., Tong, Y., Yang, D., Mao, X., and Yang, M. (2022). Flavonoids-Natural Gifts to Promote Health and Longevity. *Int J Mol Sci* **23**. 10.3390/ijms23042176.

Fatkin, D., MacRae, C., Sasaki, T., Wolff, M.R., Porcu, M., Frenneaux, M., Atherton, J., Vidaillet, H.J., Jr., Spudich, S., De Girolami, U., et al. (1999). Missense mutations in the rod domain of the lamin A/C gene as causes of dilated cardiomyopathy and conduction-system disease. *N Engl J Med* **341**, 1715-1724. 10.1056/NEJM199912023412302.

Fedorchak, G.R., Kaminski, A., and Lammerding, J. (2014). Cellular mechanosensing: getting to the nucleus of it all. *Prog Biophys Mol Biol* **115**, 76-92. 10.1016/j.pbiomolbio.2014.06.009.

Flotow, H., Graves, P.R., Wang, A.Q., Fiol, C.J., Roeske, R.W., and Roach, P.J. (1990). Phosphate Groups as Substrate Determinants for Casein Kinase-I Action. *J Biol Chem* **265**, 14264-14269.

Fuchs, E., and Weber, K. (1994). Intermediate filaments: structure, dynamics, function, and disease. *Annu Rev Biochem* **63**, 345-382. 10.1146/annurev.bi.63.070194.002021.

Gerace, L., and Blobel, G. (1980). Nuclear-Envelope Lamina Is Reversibly Depolymerized during Mitosis. *Cell* **19**, 277-287. Doi 10.1016/0092-8674(80)90409-2.

Goldman, R.D., Gruenbaum, Y., Moir, R.D., Shumaker, D.K., and Spann, T.P. (2002). Nuclear lamins: building blocks of nuclear architecture. *Genes Dev* **16**, 533-547. 10.1101/gad.960502.

Gonzalez-Cruz, R.D., Dahl, K.N., and Darling, E.M. (2018). The Emerging Role of Lamin C as an Important LMNA Isoform in Mechanophenotype. *Front Cell Dev Biol* **6**. ARTN 151

10.3389/fcell.2018.00151.

Gordon, L.B., Cao, K., and Collins, F.S. (2012). Progeria: translational insights from cell biology. *J Cell Biol* **199**, 9-13. 10.1083/jcb.201207072.

Gordon, L.B., Rothman, F.G., Lopez-Otin, C., and Misteli, T. (2014). Progeria: a paradigm for translational medicine. *Cell* **156**, 400-407. 10.1016/j.cell.2013.12.028.

Guelen, L., Pagie, L., Brasset, E., Meuleman, W., Faza, M.B., Talhout, W., Eussen, B.H., de Klein, A., Wessels, L., de Laat, W., and van Steensel, B. (2008). Domain organization of human chromosomes revealed by mapping of nuclear lamina interactions. *Nature* **453**, 948-951. 10.1038/nature06947.

Guillin-Amarelle, C., Fernandez-Pombo, A., Sanchez-Iglesias, S., and Araujo-Vilar, D. (2018). Lipodystrophic laminopathies: Diagnostic clues. *Nucleus* **9**, 249-260. 10.1080/19491034.2018.1454167.

Ha, N.C., Tonozuka, T., Stamos, J.L., Choi, H.J., and Weis, W.I. (2004). Mechanism of phosphorylation-dependent binding of APC to beta-catenin and its role in beta-catenin degradation. *Mol Cell* **15**, 511-521. 10.1016/j.molcel.2004.08.010.

Handoko, L., Xu, H., Li, G., Ngan, C.Y., Chew, E., Schnapp, M., Lee, C.W., Ye, C., Ping, J.L., Mulawadi, F., et al. (2011). CTCF-mediated functional chromatin interactome in pluripotent cells. *Nat Genet* **43**, 630-638. 10.1038/ng.857.

Heald, R., and McKeon, F. (1990). Mutations of phosphorylation sites in lamin A that prevent nuclear lamina disassembly in mitosis. *Cell* **61**, 579-589. 10.1016/0092-8674(90)90470-y.

Hebditch, M., and Warwicker, J. (2019). Web-based display of protein surface and pH-dependent properties for assessing the developability of biotherapeutics. *Sci Rep* **9**, 1969. 10.1038/s41598-018-36950-8.

Heo, L., Lee, H., and Seok, C. (2016). GalaxyRefineComplex: Refinement of protein-protein complex model structures driven by interface repacking. *Sci Rep* **6**, 32153. 10.1038/srep32153.

Herrmann, H., and Aebi, U. (2000). Intermediate filaments and their associates: multi-talented structural elements specifying cytoarchitecture and cytodynamics. *Curr Opin Cell Biol* **12**, 79-90. 10.1016/s0955-0674(99)00060-5.

Herrmann, H., and Aebi, U. (2004). Intermediate filaments: molecular structure, assembly mechanism, and integration into functionally distinct intracellular Scaffolds. *Annu Rev Biochem* **73**, 749-789. 10.1146/annurev.biochem.73.011303.073823.

Herrmann, H., and Aebi, U. (2016). Intermediate Filaments: Structure and Assembly. *Cold Spring Harb Perspect Biol* **8**. 10.1101/cshperspect.a018242.

Herrmann, H., Bar, H., Kreplak, L., Strelkov, S.V., and Aebi, U. (2007). Intermediate filaments: from cell architecture to nanomechanics. *Nat Rev Mol Cell Biol* **8**, 562-573. 10.1038/nrm2197.

Herrmann, H., Hesse, M., Reichenzeller, M., Aebi, U., and Magin, T.M. (2003). Functional complexity of intermediate filament cytoskeletons: from structure to assembly to gene ablation. *Int Rev Cytol* **223**, 83-175. 10.1016/s0074-7696(05)23003-6.

Jeong, S., Ahn, J., Jo, I., Kang, S.M., Park, B.J., Cho, H.S., Kim, Y.H., and Ha, N.C. (2022). Cyclin-dependent kinase 1 depolymerizes nuclear lamin filaments by disrupting the head-to-tail interaction of the lamin central rod domain. *J Biol Chem* **298**, 102256. 10.1016/j.jbc.2022.102256.

Jumper, J., Evans, R., Pritzel, A., Green, T., Figurnov, M., Ronneberger, O., Tunyasuvunakool, K., Bates, R., Zidek, A., Potapenko, A., et al. (2021). Highly accurate protein structure prediction with AlphaFold. *Nature* **596**, 583-589. 10.1038/s41586-021-03819-2.

Kandert, S., Luke, Y., Kleinhenz, T., Neumann, S., Lu, W., Jaeger, V.M., Munck, M., Wehnert, M., Muller, C.R., Zhou, Z., et al. (2007). Nesprin-2 giant safeguards nuclear envelope architecture in LMNA S143F progeria cells. *Hum Mol Genet* **16**, 2944-2959. 10.1093/hmg/ddm255.

Kang, S.M., Yoon, M.H., Ahn, J., Kim, J.E., Kim, S.Y., Kang, S.Y., Joo, J., Park, S., Cho, J.H., Woo, T.G., et al. (2021). Author Correction: Progerinin, an optimized progerin-lamin A binding inhibitor, ameliorates premature senescence phenotypes of Hutchinson-Gilford progeria syndrome. *Commun Biol* **4**, 297. 10.1038/s42003-021-01843-6.

Kang, S.M., Yoon, M.H., and Park, B.J. (2018). Laminopathies; Mutations on single gene and various human genetic diseases. *Bmb Rep* **51**, 327-337. 10.5483/BMBRep.2018.51.7.113.

Khan, H., Belwal, T., Efferth, T., Farooqi, A.A., Sanches-Silva, A., Vacca, R.A., Nabavi, S.F., Khan, F., Prasad Devkota, H., Barreca, D., et al. (2021). Targeting epigenetics in cancer: therapeutic potential of flavonoids. *Crit Rev Food Sci Nutr* **61**, 1616-1639. 10.1080/10408398.2020.1763910.

Kim, K., Cha, J.S., Kim, J.S., Ahn, J., Ha, N.C., and Cho, H.S. (2018). Crystal structure of GSK3beta in complex with the flavonoid, morin. *Biochem Biophys Res Commun* **504**, 519-524. 10.1016/j.bbrc.2018.08.182.

Kinoshita, E., Kinoshita-Kikuta, E., and Koike, T. (2012). Phos-tag SDS-PAGE systems for phosphorylation profiling of proteins with a wide range of

molecular masses under neutral pH conditions. *Proteomics* **12**, 192-202. 10.1002/pmic.201100524.

Kirschner, J., Brune, T., Wehnert, M., Denecke, J., Wasner, C., Feuer, A., Marquardt, T., Ketelsen, U.P., Wieacker, P., Bonnemann, C.G., and Korinthenberg, R. (2005). p.S143F mutation in lamin A/C: a new phenotype combining myopathy and progeria. *Ann Neurol* **57**, 148-151. 10.1002/ana.20359.

Kochin, V., Shimi, T., Torvaldson, E., Adam, S.A., Goldman, A., Pack, C.G., Melo-Cardenas, J., Imanishi, S.Y., Goldman, R.D., and Eriksson, J.E. (2014). Interphase phosphorylation of lamin A. *J Cell Sci* **127**, 2683-2696. 10.1242/jcs.141820.

Krimm, I., Ostlund, C., Gilquin, B., Couprie, J., Hossenlopp, P., Mornon, J.P., Bonne, G., Courvalin, J.C., Worman, H.J., and Zinn-Justin, S. (2002). The Ig-like structure of the C-terminal domain of lamin A/C, mutated in muscular dystrophies, cardiomyopathy, and partial lipodystrophy. *Structure* **10**, 811-823. 10.1016/s0969-2126(02)00777-3.

Lazarides, E. (1980). Intermediate Filaments as Mechanical Integrators of Cellular Space. *Nature* **283**, 249-256. DOI 10.1038/283249a0.

Lee, S.J., Jung, Y.S., Yoon, M.H., Kang, S.M., Oh, A.Y., Lee, J.H., Jun, S.Y., Woo, T.G., Chun, H.Y., Kim, S.K., et al. (2016). Interruption of progerin-lamin A/C binding ameliorates Hutchinson-Gilford progeria syndrome phenotype. *J Clin Invest* **126**, 3879-3893. 10.1172/JCI84164.

Lilina, A.V., Chernyatina, A.A., Guzenko, D., and Strelkov, S.V. (2020). Lateral A11 type tetramerization in lamins. *J Struct Biol* **209**, 107404. 10.1016/j.jsb.2019.10.006.

Liu, S.Y., and Ikegami, K. (2020). Nuclear lamin phosphorylation: an emerging role in gene regulation and pathogenesis of laminopathies. *Nucleus* **11**, 299-314. 10.1080/19491034.2020.1832734.

Lopez-Soler, R.I., Moir, R.D., Spann, T.P., Stick, R., and Goldman, R.D. (2001). A role for nuclear lamins in nuclear envelope assembly. *J Cell Biol* **154**, 61-70. 10.1083/jcb.200101025.

Machiels, B.M., Zorenc, A.H., Endert, J.M., Kuijpers, H.J., van Eys, G.J., Ramaekers, F.C., and Broers, J.L. (1996). An alternative splicing product of the lamin A/C gene lacks exon 10. *J Biol Chem* **271**, 9249-9253. 10.1074/jbc.271.16.9249.

Machowska, M., Piekarowicz, K., and Rzepecki, R. (2015). Regulation of lamin properties and functions: does phosphorylation do it all? *Open Biol* **5**. 10.1098/rsob.150094.

Mahen, R., Hattori, H., Lee, M., Sharma, P., Jeyasekharan, A.D., and Venkitaraman, A.R. (2013). A-type lamins maintain the positional stability of DNA damage repair foci in mammalian nuclei. *PLoS One* **8**, e61893. 10.1371/journal.pone.0061893.

Makarov, A.A., Zou, J., Houston, D.R., Spanos, C., Solovyova, A.S., Cardenal-Peralta, C., Rappsilber, J., and Schirmer, E.C. (2019). Lamin A molecular compression and sliding as mechanisms behind nucleoskeleton elasticity. *Nat Commun* **10**, 3056. 10.1038/s41467-019-11063-6.

Marcelot, A., Worman, H.J., and Zinn-Justin, S. (2020). Protein structural and mechanistic basis of progeroid laminopathies. *FEBS J*. 10.1111/febs.15526.

Marcelot, A., Worman, H.J., and Zinn-Justin, S. (2021). Protein structural and mechanistic basis of progeroid laminopathies. *FEBS J* **288**, 2757-2772. 10.1111/febs.15526.

McKeon, F. (1991). Nuclear lamin proteins: domains required for nuclear targeting, assembly, and cell-cycle-regulated dynamics. *Curr Opin Cell Biol* **3**, 82-86. 10.1016/0955-0674(91)90169-y.

McKeon, F.D., Kirschner, M.W., and Caput, D. (1986). Homologies in both primary and secondary structure between nuclear envelope and intermediate filament proteins. *Nature* **319**, 463-468. 10.1038/319463a0.

McPherson, E., Turner, L., Zador, I., Reynolds, K., Macgregor, D., and Giampietro, P.F. (2009). Ovarian Failure and Dilated Cardiomyopathy Due to a Novel Lamin Mutation. *Am J Med Genet A* **149a**, 567-572. 10.1002/ajmg.a.32627.

Meggio, F., Perich, J.W., Reynolds, E.C., and Pinna, L.A. (1991). A Synthetic Beta-Casein Phosphopeptide and Analogs as Model Substrates for Casein Kinase-1, a Ubiquitous, Phosphate Directed Protein-Kinase. *Febs Lett* **283**, 303-306. Doi 10.1016/0014-5793(91)80614-9.

Muchir, A., Medioni, J., Laluc, M., Massart, C., Arimura, T., van der Kooi, A.J., Desguerre, I., Mayer, M., Ferrer, X., Briault, S., et al. (2004). Nuclear envelope alterations in fibroblasts from patients with muscular dystrophy, cardiomyopathy, and partial lipodystrophy carrying lamin A/C gene mutations. *Muscle Nerve* **30**, 444-450. 10.1002/mus.20122.

Murray-Nerger, L.A., and Cristea, I.M. (2021). Lamin post-translational modifications: emerging toggles of nuclear organization and function. *Trends Biochem Sci* **46**, 832-847. 10.1016/j.tibs.2021.05.007.

Omary, M.B., Ku, N.O., Tao, G.Z., Toivola, D.M., and Liao, J. (2006). 'Heads and tails' of intermediate filament phosphorylation: multiple sites and functional insights. *Trends Biochem Sci* **31**, 383-394. 10.1016/j.tibs.2006.05.008.

Osmanagic-Myers, S., Dechat, T., and Foisner, R. (2015). Lamins at the crossroads of mechanosignaling. *Gene Dev* **29**, 225-237. 10.1101/gad.255968.114.

Otwinowski, Z., and Minor, W. (1997). Processing of X-ray diffraction data collected in oscillation mode. *Methods Enzymol* **276**, 307-326.

Panche, A.N., Diwan, A.D., and Chandra, S.R. (2016). Flavonoids: an overview. *J Nutr Sci* **5**, e47. 10.1017/jns.2016.41.

Parry, D.A. (2006). Hendecad repeat in segment 2A and linker L2 of intermediate filament chains implies the possibility of a right-handed coiled-coil structure. *J Struct Biol* **155**, 370-374. 10.1016/j.jsb.2006.03.017.

Peter, M., Nakagawa, J., Doree, M., Labbe, J.C., and Nigg, E.A. (1990). In vitro disassembly of the nuclear lamina and M phase-specific phosphorylation of lamins by cdc2 kinase. *Cell* **61**, 591-602. 10.1016/0092-8674(90)90471-p.

Pethig, K., Genschel, J., Peters, T., Wilhelmi, M., Flemming, P., Lochs, H., Haverich, A., and Schmidt, H.H. (2005). LMNA mutations in cardiac transplant recipients. *Cardiology* **103**, 57-62. 10.1159/000082048.

Piekarowicz, K., Machowska, M., Dzianisava, V., and Rzepecki, R. (2019). Hutchinson-Gilford Progeria Syndrome-Current Status and Prospects for Gene Therapy Treatment. *Cells* **8**. 10.3390/cells8020088.

Pollex, R.L., and Hegele, R.A. (2004). Hutchinson-Gilford progeria syndrome. *Clin Genet* **66**, 375-381. 10.1111/j.1399-0004.2004.00315.x.

Prokocimer, M., Davidovich, M., Nissim-Rafinia, M., Wiesel-Motiuk, N., Bar, D.Z., Barkan, R., Meshorer, E., and Gruenbaum, Y. (2009). Nuclear lamins: key regulators of nuclear structure and activities. *J Cell Mol Med* **13**, 1059-1085. 10.1111/j.1582-4934.2008.00676.x.

Pronk, S., Pall, S., Schulz, R., Larsson, P., Bjelkmar, P., Apostolov, R., Shirts, M.R., Smith, J.C., Kasson, P.M., van der Spoel, D., et al. (2013). GROMACS

4.5: a high-throughput and highly parallel open source molecular simulation toolkit. *Bioinformatics* **29**, 845-854. 10.1093/bioinformatics/btt055.

Puttaraju, M., Jackson, M., Klein, S., Shilo, A., Bennett, C.F., Gordon, L., Rigo, F., and Misteli, T. (2021). Systematic screening identifies therapeutic antisense oligonucleotides for Hutchinson-Gilford progeria syndrome. *Nat Med* **27**, 526-535. 10.1038/s41591-021-01262-4.

Qi, Y.F., Cheng, X., Han, W., Jo, S., Schulten, K., and Im, W. (2014). CHARMM-GUI PACE CG Builder for Solution, Micelle, and Bilayer Coarse-Grained Simulations. *J Chem Inf Model* **54**, 1003-1009. 10.1021/ci500007n.

Ramesh, P., Jagadeesan, R., Sekaran, S., Dhanasekaran, A., and Vimalraj, S. (2021). Flavonoids: Classification, Function, and Molecular Mechanisms Involved in Bone Remodelling. *Front Endocrinol* **12**. ARTN 779638

10.3389/fendo.2021.779638.

Rankin, J., and Ellard, S. (2006). The laminopathies: a clinical review. *Clin Genet* **70**, 261-274. 10.1111/j.1399-0004.2006.00677.x.

Rufino, A.T., Costa, V.M., Carvalho, F., and Fernandes, E. (2021). Flavonoids as antiobesity agents: A review. *Med Res Rev* **41**, 556-585. 10.1002/med.21740.

Schrodinger, LLC (2015). The PyMOL Molecular Graphics System, Version 1.8.

Shimi, T., Butin-Israeli, V., Adam, S.A., and Goldman, R.D. (2010). Nuclear lamins in cell regulation and disease. *Cold Spring Harb Symp Quant Biol* **75**, 525-531. 10.1101/sqb.2010.75.045.

Simon, D.N., and Wilson, K.L. (2013). Partners and post-translational modifications of nuclear lamins. *Chromosoma* **122**, 13-31. 10.1007/s00412-013-0399-8.

Stalmans, G., Lilina, A.V., Vermeire, P.J., Fiala, J., Novak, P., and Strelkov, S.V. (2020). Addressing the Molecular Mechanism of Longitudinal Lamin Assembly Using Chimeric Fusions. *Cells* **9**. 10.3390/cells9071633.

Steinert, P.M., Marekov, L.N., and Parry, D.A. (1993). Diversity of intermediate filament structure. Evidence that the alignment of coiled-coil molecules in vimentin is different from that in keratin intermediate filaments. *J Biol Chem* **268**, 24916-24925.

Stuurman, N., Heins, S., and Aebi, U. (1998). Nuclear lamins: their structure, assembly, and interactions. *J Struct Biol* **122**, 42-66. 10.1006/jsbi.1998.3987.

Swift, J., Ivanovska, I.L., Buxboim, A., Harada, T., Dingal, P.C.D.P., Pinter, J., Pajerowski, J.D., Spinler, K.R., Shin, J.W., Tewari, M., et al. (2013). Nuclear Lamin-A Scales with Tissue Stiffness and Enhances Matrix-Directed Differentiation. *Science* **341**. ARTN 124010410.1126/science.1240104.

Turgay, Y., Eibauer, M., Goldman, A.E., Shimi, T., Khayat, M., Ben-Harush, K., Dubrovsky-Gaupp, A., Sapra, K.T., Goldman, R.D., and Medalia, O. (2017). The molecular architecture of lamins in somatic cells. *Nature* **543**, 261-264. 10.1038/nature21382.

Turgay, Y., and Medalia, O. (2017). The structure of lamin filaments in somatic cells as revealed by cryo-electron tomography. *Nucleus* **8**, 475-481. 10.1080/19491034.2017.1337622.

Vahabikashi, A., Sivagurunathan, S., Nicdao, F.A.S., Han, Y.L., Park, C.Y., Kittisopikul, M., Wong, X., Tran, J.R., Gundersen, G.G., Reddy, K.L., et al. (2022). Nuclear lamin isoforms differentially contribute to LINC complex-dependent nucleocytoskeletal coupling and whole-cell mechanics. *Proc Natl Acad Sci U S A* **119**, e2121816119. 10.1073/pnas.2121816119.

Vermeire, P.J., Stalmans, G., Lilina, A.V., Fiala, J., Novak, P., Herrmann, H., and Strelkov, S.V. (2021). Molecular Interactions Driving Intermediate Filament Assembly. *Cells* **10**. 10.3390/cells10092457.

Wang, H., Guo, Y., Luo, Z., Gao, L., Li, R., Zhang, Y., Kalaji, H.M., Qiang, S., and Chen, S. (2022). Recent Advances in Alternaria Phytotoxins: A Review of Their Occurrence, Structure, Bioactivity, and Biosynthesis. *J Fungi (Basel)* **8**. 10.3390/jof8020168.

Ward, G.E., and Kirschner, M.W. (1990). Identification of cell cycle-regulated phosphorylation sites on nuclear lamin C. *Cell* **61**, 561-577. 10.1016/0092-8674(90)90469-u.

Willaume, S., Rass, E., Fontanilla-Ramirez, P., Moussa, A., Wanschoor, P., and Bertrand, P. (2021). A Link between Replicative Stress, Lamin Proteins, and Inflammation. *Genes-Basel* **12**. ARTN 55210.3390/genes12040552.

Winn, M.D., Ballard, C.C., Cowtan, K.D., Dodson, E.J., Emsley, P., Evans, P.R., Keegan, R.M., Krissinel, E.B., Leslie, A.G., McCoy, A., et al. (2011). Overview of the CCP4 suite and current developments. *Acta Crystallogr D Biol Crystallogr* **67**, 235-242. 10.1107/S0907444910045749.

Xie, W., Chojnowski, A., Boudier, T., Lim, J.S., Ahmed, S., Ser, Z., Stewart, C., and Burke, B. (2016). A-type Lamins Form Distinct Filamentous Networks with Differential Nuclear Pore Complex Associations. *Curr Biol* **26**, 2651-2658. 10.1016/j.cub.2016.07.049.

Xu, D., Hu, M.J., Wang, Y.Q., and Cui, Y.L. (2019). Antioxidant Activities of Quercetin and Its Complexes for Medicinal Application. *Molecules* **24**. 10.3390/molecules24061123.

Young, S.G., Meta, M., Yang, S.H., and Fong, L.G. (2006). Prelamin A farnesylation and progeroid syndromes. *J Biol Chem* **281**, 39741-39745. 10.1074/jbc.R600033200.

Yousefzadeh, M.J., Zhu, Y., McGowan, S.J., Angelini, L., Fuhrmann-Stroissnigg, H., Xu, M., Ling, Y.Y., Melos, K.I., Pirtskhalava, T., Inman, C.L., et al. (2018). Fisetin is a senotherapeutic that extends health and lifespan. *Ebiomedicine* **36**, 18-28. 10.1016/j.ebiom.2018.09.015.

국문초록

세포핵 중간세사 라민은 핵의 형태를 유지하고 외부의 기계적 자극으로부터 대항하는 힘을 갖는 3 차원 그물망 구조를 형성한다. 핵 라민은 세포의 생명유지에 중요하다. 라민은 유전자 돌연변이에 의해 다양한 laminopathies 가 나타나는데, 그 중 S143F 의 유전자 돌연변이는 프로게리아와 근육 파괴를 모두 특징으로 하는 표현형을 유발한다. 본 연구에서는 S143F 변이를 가진 라민 A/C 의 단백질 결정 구조를 규명하였다. 라민 A/C S143F 의 구조에서 페닐알라닌으로 치환된 143 번 잔기는 소수성 상호작용에 의해 결정구조에서 사량체의 코일들 사이의 X 자형 상호작용을 보여주었다. 후속연구는 필라멘트 사이의 X 자형 상호작용이 정상적인 라민 그물망 구조를 방해하는데 중요한 역할을 한다는 것을 보여주었다. 이 연구 결과는 3 차원 그물 구조의 조립 메커니즘을 제안하고 핵 변형에 의해 노화과정을 이해하기 위한 분자적 수준의 토대를 추가로 제공한다.

핵 라민은 A11 과 A22 결합 방법으로 알려진 코일형 이량체의 두가지 분자 배열을 통해 길고 선형의 필라멘트를 형성함으로써 핵의 구조를 유지한다. 라민의 사량체 형성과정에서 A11 과 A22 와 결합하는 코일형 이중체 사이의 결합은 ACN 결합이라는 또다른 평행한 코일 1a 와 코일 2 의 카르복실 말단 사이의 머리-꼬리 상호작용을 형성한다. 체세포분열 동안 CDK1 인산화효소 복합체에 의해 라민의 아미노 말단의 머리 부분의 인산화는 핵 라민의 해체를 유발하지만, 이에 관한 분자수준의 메커니즘은 알려지지 않은 상태로 남아있다. 본 연구에서는 정제된 단백질을 이용하여 CDK1 복합체에 의한 인산화는 코일 1a 와 코일 2 의 C-말단 사이의 ACN 결합을 직접적으로 방해함으로써 섬유질 라민의 분해를 촉진한다는 것을

밝혔다. 또한 코일 1a 와 코일 2 사이의 결합이 아미노산 잔기간의 이온 결합력의 변화로 인해 중단되었음을 관찰하였습니다. 덧붙여 분자모델을 곁들여 라민이 CDK1 에 의존한 해체 메커니즘을 제시하였다.

L59R 돌연변이에 의한 laminopathy 는 근육파괴질환에서 골격근육질병과 심장근육병증의 표현형을 모두 유발한다. 이 유전자 돌연변이는 coil 1a 의 안정도를 변화시켜 ACN 결합을 강하게 유도하며, 이는 인산화효소에 의한 라민의 해체 시도를 저지할 정도로 강력하다는 것을 앞서 실험을 통해 확인하였다. 본 연구에서는 이 결합을 억제하는 천연물을 스크리닝 하였고 플라보노이드 계열의 모린, 바이칼레인, 피세틴, 그리고 아피제닌을 선정하였다. 분자 도킹과 분자 동력학 시뮬레이션을 활용하여 이들의 분자적 작동기전에 대한 단서를 제공하였다. 그리고 HT1080 세포 기반 분석은 라민 A 의 비정상적 상호작용에 플라보노이드가 효과적인 분자로서 활용 가능성을 보여주었다. 이러한 결과들은 라민의 유전질병에서 플라보노이드가 항산화 기능 외에 단백질의 결합방해에 직접적으로 관여하여 치료제로서의 활용 가능성을 보여준다.

주요어: 중간세사, 핵라민 A/C, 라민유래질병, 인산화, 단백질 결정구조, 플라보노이드

학번: 2017-29613